Sedimentary Geology 433 (2022) 106122

Contents lists available at ScienceDirect

Sedimentary Geology

journal homepage: www.elsevier.com/locate/sedgeo

Variations in water discharge at different temporal scales in a mud-prone alluvial succession: The Paleocene-Eocene of the Tremp-Graus Basin, Spain

Oscar J. Arévalo [a], Luca Colombera [a,*], Nigel P. Mountney [a], Giorgio Basilici [b,c], Marcus V.T. Soares [b]

[a] Fluvial, Eolian & Shallow-Marine Research Group, School of Earth and Environment, University of Leeds, Leeds, UK
[b] Geosciences Institute, State University of Campinas, Campinas, Brazil
[c] Centro Regional de Investigaciones Científicas y Transferencia Tecnológica, CONICET, La Rioja, Argentina

ARTICLE INFO

Article history:
Received 6 January 2022
Received in revised form 3 March 2022
Accepted 7 March 2022
Available online 12 March 2022

Editor: Dr. Catherine Chagué

Keywords:
Fluvial architecture
Discharge variability
upper flow regime
Unconfined flows
Paleocene-Eocene Thermal Maximum
PETM

ABSTRACT

The late Paleocene to earliest Eocene sedimentary record in the eastern Tremp-Graus Basin (southern Pyrenees, Spain) consists of a mud-prone fluvial succession informally known as 'Upper Red Garumnian', which is dominantly composed of non-channelized deposits interspersed with fluvial channel bodies. The succession records evidence of variations in water discharge at multiple temporal scales. One-hundred-and-eighty sand-prone and conglomeratic bodies present within otherwise fine-grained deposits have been examined by facies and architectural-element analyses. These have been assigned to four distinctive types: (i) simple and (ii) compound channelized deposits, (iii) multilateral and multistorey elements, and (iv) sediment gravity-flow deposits. Simple and compound channel bodies represent deposits of channelized high-energy flows associated respectively with single floods or multiple events occurring in the same channel belt. Multilateral and multistorey elements are associated with sedimentation in longer-lived channel belts. An increase in the occurrence of these latter elements through the stratigraphy can be related to changes in tectonic and/or climatic drivers, heralding a change in facies architecture that signifies a shift to perennial discharge conditions and incised-valley backfilling. This is itself followed by a marked change in architectural style in a part of stratigraphy recording the Paleocene-Eocene Thermal Maximum (PETM), when variations in precipitation regime and/or intrabasinal characteristics (e.g., vegetation) related to this event favoured the lateral migration of channels, causing the development of laterally extensive coarse-grained bodies. Floodplain sediments comprise (i) heterolithic deposits accumulated in the vicinities of the fluvial channels where riparian ecosystems were developed, and (ii) overbank mudstones with variable degree of pedogenesis, especially associated with wetting and drying cycles in areas of the floodplain located distally away from fluvial channels. This succession records the importance of water-discharge variations in the evolution of alluvial systems: it displays facies arrangements recording the effects of highly variable discharge in ephemeral to perennial channels, as well as variations in stratigraphic architecture testifying to longer-term hydrological changes in the late Paleocene and earliest Eocene.

1. Introduction

The facies record of water discharge variability in fluvial successions has long been a debated research topic. For example, many early studies of present-day and recent ephemeral stream floods in arid areas described a great variety of sedimentary structures indicating both upper- and lower-flow regime sedimentation in the resulting deposits (e.g., Williams, 1971; Karcz, 1972; Picard and High, 1973), whereas other authors conversely reported a significant predominance of horizontal stratification in deposits of similar origin (e.g., McKee et al., 1967; Frostick and Reid, 1977). Similarly, in the rock record, some successions interpreted as the product of ephemeral streams are dominated by horizontal lamination (Tunbridge, 1981), whereas many others display a wider variety of structures and architectural arrangements indicative of variable flow regimes (Wells, 1983; Stear, 1985; Olsen, 1989; Bromley, 1991; North and Taylor, 1996; Soares et al., 2021). Such variability, in terms of sedimentary structures and architectures, suggests that any interpretation of ephemeral or perennial flow based on particular lithofacies arrangements are inherently uncertain (cf. Colombera and Mountney, 2019), and that consideration should be given to specific evidence of streambed drying (e.g., mudcracks, root marks, burrows) (Bridge and Demicco, 2008).

* Corresponding author.
E-mail address: l.colombera@leeds.ac.uk (L. Colombera).

https://doi.org/10.1016/j.sedgeo.2022.106122

Nonetheless, the role of discharge variability as a fundamental control on the resultant facies architecture of river systems is increasingly emphasized (Fielding et al., 2009, 2018; Plink-Björklund, 2015; Leary and Ganti, 2020). In this perspective, new categories of fluvial systems between the perennial and ephemeral end-members are considered, including for example strongly seasonal rivers with intermittent fluvial channels, as described by Allen et al. (2014). The recognition of relevant sedimentary features that can be referred to for characterizing different types of successions in terms of discharge variability allows the re-evaluation of ancient fluvial successions and their palaeohydraulic and palaeoclimatic interpretations. This is particularly relevant to fluvial systems that may not necessarily be located in ancient arid or monsoonal regions, where discharge variability is expected, but rather in subtropical or temperate zones where strongly seasonal conditions may be favoured by local climatic, palaeogeographic and/or orographic characteristics. Thus, the water discharge variability of alluvial systems is related to extrinsic (allogenic) controls on sedimentation, particularly climate and tectonics, which can ultimately control the evolution and facies architecture of a fluvial system. In cases where the timing and magnitude with which these allogenic drivers operate can be inferred thanks to available geological constraints, it becomes possible to evaluate the architectural record of such extrinsic controls.

In the eastern part of the Tremp-Graus basin (southern Pyrenees, Spain), and specifically in the Arén and Esplugafreda sectors, there exist laterally continuous exposures of a fluvial succession described as dominantly being the product of ephemeral rivers (Dreyer, 1993). This succession, informally named as Upper Red Garumnian (Rosell et al., 2001), spans the transition between the Paleocene and Eocene, and has been the focus of numerous studies that aimed to define a general sedimentological and stratigraphic framework (e.g., Médus and Colombo, 1991; Cuevas, 1992; Dreyer, 1993; Pujalte and Schmitz, 2005; López-Martínez et al., 2006b). From a more regional perspective, the study of the structural evolution of the Pyrenees, together with the application of geochronological techniques, has allowed the definition of different stages of tectonic uplift and the influence of such uplift on the sedimentation of the entire Late Cretaceous to Miocene synorogenic succession (e.g. Cámara and Klimowitz, 1985; Puigdefàbregas et al., 1992; Ardèvol et al., 2000; Whitchurch et al., 2011). Additionally, with the identification of a negative carbon isotopic excursion associated with the Paleocene-Eocene Thermal Maximum (PETM; Schmitz and Pujalte, 2003), this succession has been the focus of studies on the stratigraphic identification of this hyperthermal event, and on the associated environmental responses preserved in the sedimentary record (Manners et al., 2013; Dawson et al., 2014; Adatte et al., 2014; Pujalte et al., 2014; Colombera et al., 2017; Chen et al., 2018; Duller et al., 2019). Previous local studies from the Arén and Esplugafreda exposures have documented evidences of pedogenic and diagenetic processes (Fjellbirkeland, 1990), palaeofloras (Médus and Colombo, 1991), and the records of depositional environments and external controlling factors on sedimentation (Dreyer, 1993).

The aim of this study is to leverage on the excellent exposures at these localities to present detailed qualitative and quantitative descriptions of this fluvial succession, and to document sedimentary features at different scales (macroscopic to megascopic), to enable inferences of the effects of variations in river discharge at different temporal scales (from that of a single flash flood to the order of 10^5 yr). In addition, by building on current knowledge of the tectonic evolution of the Pyrenees, and of climatic conditions at the Paleocene-Eocene transition, this study assesses the evolutionary response of this fluvial system under constrained sets of allogenic conditions. Specific research objectives are as follows: (i) to document the geometry and internal lithofacies arrangement of the architectural elements of this succession, and vertical trends thereof, using techniques in lithofacies- and architectural-element analyses; (ii) to quantify the geometry of coarse-grained (arenaceous and conglomeratic) bodies by integrating data from orthophotographs, LiDAR DEMs, field photomosaics and ground-based GPS measurements; (iii) and to interpret formative sedimentary processes, depositional sub-environments, and variations in environmental conditions through the stratigraphy.

2. Geological setting

The Pyrenean mountain chain is an asymmetric fold-and-thrust belt oriented in WNW-ESE direction, which extends for ~400 km between France and the Iberian Peninsula (Fig. 1A) (Choukroune, 1992; Bond and McClay, 1995; Ardèvol et al., 2000; Sibuet et al., 2004). This orogenic chain comprises an axial zone of Hercynian rocks, two oppositely verging tectonic wedges (the North Pyrenean Zone and the South Pyrenean Units), and two peripheral foreland basins, the Aquitanian and Ebro basins to the north and south, respectively (Choukroune, 1992; Capote et al., 2002; Naylor and Sinclair, 2008). The South Pyrenean Units constitute a south-verging tectonic wedge, which is transversally divided by the Pamplona and Segre oblique wrench faults into Basque (western), Tremp-Jaca-Pamplona (central) and Cadi (eastern) units (Luterbacher et al., 1991; Costa et al., 1996; Rosell et al., 2001). The Tremp-Jaca-Pamplona unit, itself, contains an easternmost part named as Central South Pyrenean Unit (CSPU) whose western boundary corresponds to the N-S to NW-SE trending Sobrarbe oblique fold-and-thrust system (Fig. 1B) (Cámara and Klimowitz, 1985; Capote et al., 2002; Fernández et al., 2012). The CSPU is a type of piggyback thrust system (Butler, 1982), which itself comprises three main WNW-ESE oriented thrust systems detached over Triassic evaporitic and argillaceous rock units. From north to south and top to bottom (Fig. 1B), these are the Bóixols (Bo), Montsec (Mo) and Serres Marginals (SM) thrust systems (Teixell and Muñoz, 2000; Capote et al., 2002; Fernández et al., 2012). On the Montsec thrust sheet, a broad syncline forms a piggyback basin known as Tremp-Graus basin (TGB), which contains a mixed clastic and calcareous sedimentary fill of Paleocene to Eocene age (Ori and Friend, 1984; Nijman, 1998; Capote et al., 2002).

The study area is located in the northern-central sector of the Tremp-Graus Basin, between the localities of Arén and Esplugafreda (Fig. 1C). The stratigraphic interval of interest is part of a mainly fine-grained and red-coloured succession that extends across a wide part of the eastern Pyrenean domain, and which has been named as 'Garumnian' (Leymerie, 1868; Rosell et al., 2001), Tremp Formation (Mey et al., 1968) or Tremp Group (Cuevas, 1992). Although the rank of group better reflects the complexity of this unit (Pujalte and Schmitz, 2005), the lack of consistency in distinguishing the different formations within the Tremp Group has precluded the widespread adoption of this term (Riera et al., 2009). Herein, the informal lithostratigraphic nomenclature of Rosell et al. (2001) is adopted, which translates to the Tremp Group subunits of Cuevas (1992) as follows: the 'Grey Garumnian' is equivalent to the Posa Formation; the 'Lower Red Garumnian' to the Conques and Talarn formations, and the 'Upper Red Garumnian' to the Esplugafreda and Claret formations (Riera et al., 2009).

The interval discussed here is the 'Upper Red Garumnian', which is a fluvial succession dominantly composed of calciclastic, mainly red-coloured mudrocks, locally banded due to pedogenic processes, and which contain calciclastic sandstone and conglomeratic bodies. Massive to crudely nodular pedogenic carbonates (calcrete) are present, though only locally. The upper part of the succession, which corresponds to the Claret Formation of Baceta et al. (2011) and Pujalte et al. (2014), locally contains a lower part (informal 'member 1' of the abovementioned authors) corresponding to local incised valley fills, which are overlain by an interval dominantly composed of amalgamated conglomeratic bodies ('member 2'). This latter interval, also named as the Claret Conglomerate by Pujalte and Schmitz (2005), has been interpreted as a megafan deposit, and covers an area of over 500 km^2 (Schmitz and Pujalte, 2007). The lower contact of the Upper Red Garumnian is not exposed in the study area, but across the Tremp-Graus basin this unit overlies an important stratigraphic surface marked locally by a palaeosol *catena*

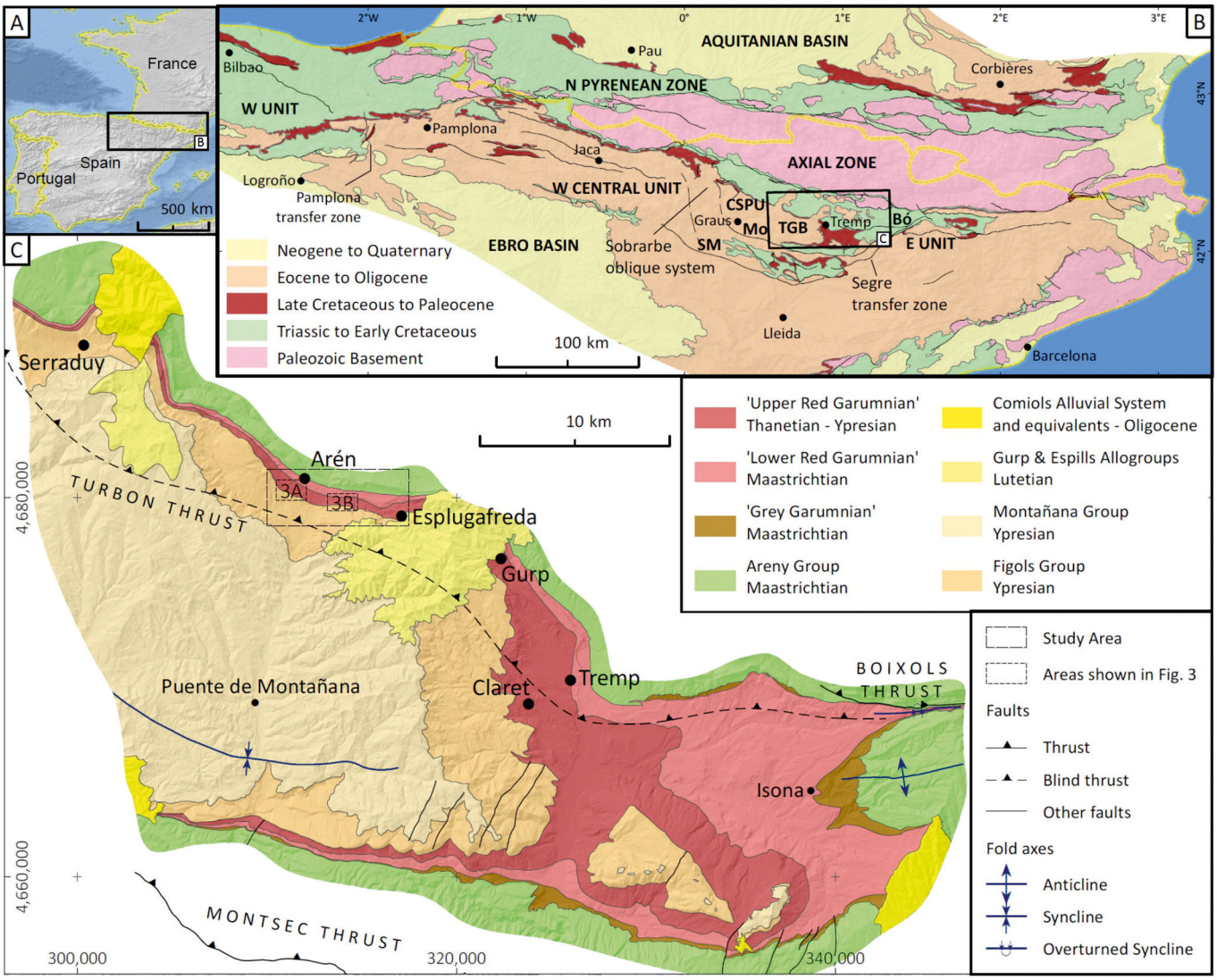

Fig. 1. Location figure. A) Location of the Pyrenean mountain system in western Europe. B) Generalized geological map of the Pyrenees westward of Bilbao, showing the main geological units, structures and tectonic elements. Abbreviations are as follows: CSPU = Central South Pyrenean Unit; TGB = Tremp-Graus Basin; Thrust sheets: Bó = Bóixols, Mo = Montsec, SM = Serres Marginals. Adapted from Capote et al. (2002). C) Generalized geological map of the eastern part of the Tremp-Graus basin, westward of Serraduy. Adapted from Ardèvol et al. (2000) and cartography by Instituto Geológico y Minero de España and Institut Cartogràfic i Geològic de Catalunya.

known as the Colmenar-Tremp Horizon (Luterbacher et al., 1991; López-Martínez et al., 2006a). The top of the Upper Red Garumnian corresponds to a transitional contact with a succession of calcareous and terrigenous marine sediments, which across the study area comprises a basal interval of fossiliferous limestones referred to in the literature as 'Alveolina Limestone' (Serra-Kiel et al., 1994, and references therein).

Well-drained and oxidizing substrate conditions prevailed during most of the Upper Red Garumnian deposition, resulting in a dominant (though not exclusively) red colour for the preserved succession. Due to these conditions, the palaeontological record of the Upper Red Garumnian is very limited; across the Tremp-Graus Basin, macro and microfossils are only found locally. Fossils and related features comprise palynomorphs (Médus, 1977; Médus and Colombo, 1991; Tremp and Esplugafreda sections, respectively), charophytes (Feist and Colombo, 1983; Claret section), mammals (López-Martinez and Peláez-Campomanes, 1999; Tremp area) and eggshells (Donaire and López-Martínez, 2009; Claret section). Palynomorphs from the Esplugafreda section allow attribution of this succession to the shallow benthic biozones *Alveolina levis* (SBZ4) to *A. ellipsoidalis* (SBZ6) (Médus and Colombo, 1991). Palynomorphs and charophytes from the Claret section are assigned to the intervals *A. primaeva* (SBZ3) to *A. cucumiformis* (SBZ5) (Médus, 1977; Feist and Colombo, 1983). Based on the biozonation scheme of Serra-Kiel et al. (1998) and the timescale of Gradstein et al. (2008), these biozones comprise the Thanetian (Paleocene) to earliest Ypresian (Eocene) (Fig. 2).

3. Methodology

This study combines results from two main activities: (i) photo-interpretation of remotely sensed imagery; and (ii) acquisition of sedimentological data in the field. Photointerpretation was undertaken on different sets of publicly available remote-sensing imagery (National Geographic Institute of Spain; Geographic and Geologic Institute of Catalonia). These datasets included high-resolution orthophotographs (horizontal resolution: 2.5 m) and Light Detection and Ranging (LiDAR) topographic data (horizontal resolution: 0.5 point/m^2). The chosen LiDAR dataset, which included a predetermined classification, was filtered to use only ground and model key points to generate a Digital Elevation Model (DEM). A DEM with pixel size of 2 m was

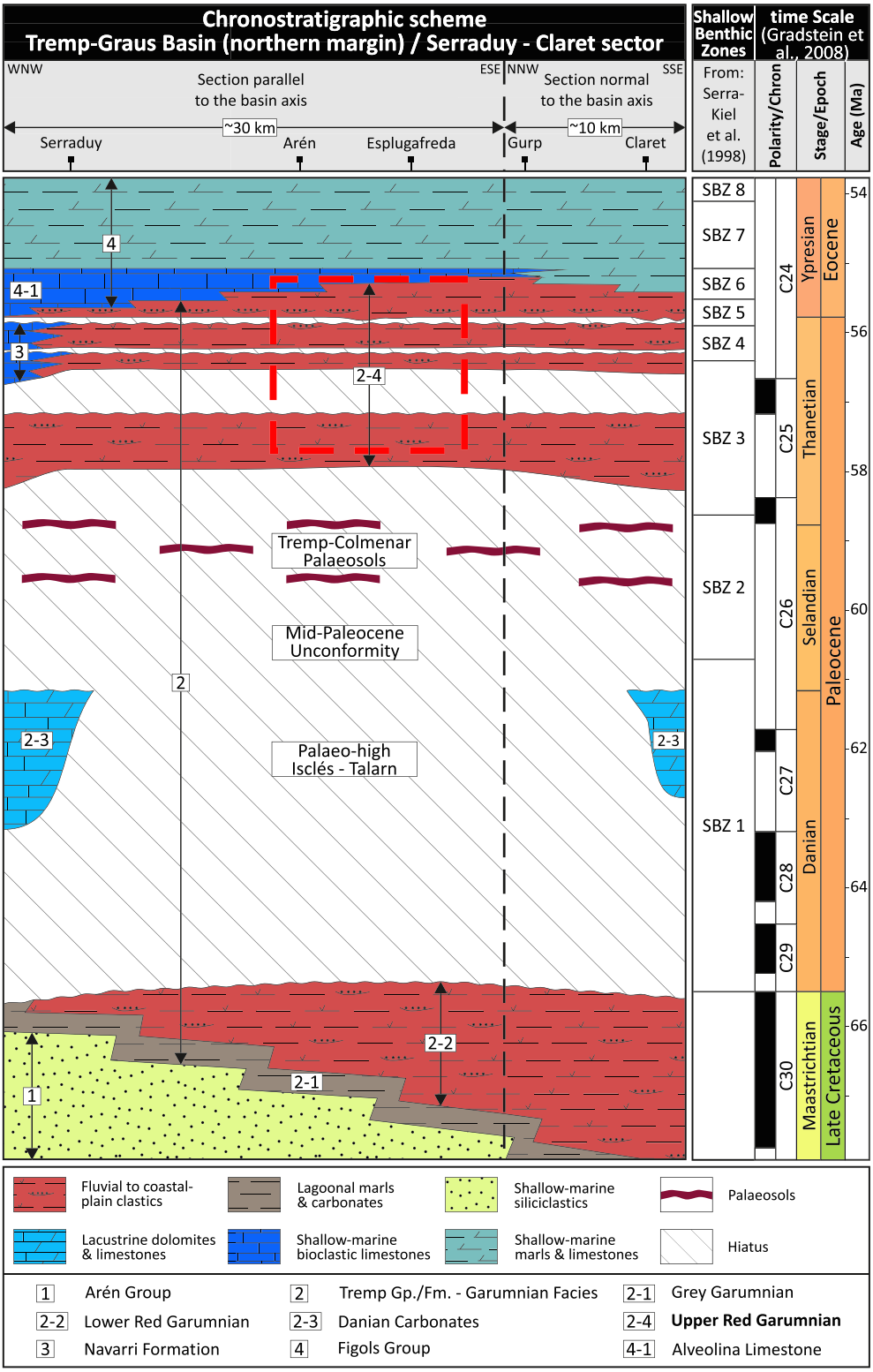

Fig. 2. Chronostratigraphic scheme of the 'Upper Red Garumnian' and correlative units in the northern part of the Tremp-Graus basin. Based on information from: Feist and Colombo (1983); Médus and Colombo (1991); Serra-Kiel et al. (1994); Vergés et al. (1995); Rosell et al. (2001); López-Martínez et al. (2006b); Arostegi et al. (2011); Whitchurch et al. (2011); Fernández et al. (2012); Manners et al. (2013); Pujalte et al. (2014). Chronostratigraphy of Gradstein et al. (2008).

generated. Through application of a gradient filter, the channelized elements, which show steeper slopes than the surrounding mudrocks, were highlighted to facilitate their mapping. Based on a combination of the processed DEM with high-resolution orthophotographs and field photomosaics, 220 channelized elements were identified and digitized.

The field work was undertaken to acquire quantitative and qualitative sedimentological data on channelized elements and floodplain

deposits. Following the methodology of Kjemperud et al. (2008), channelized elements of thickness greater than 0.5 m were identified and mapped. To characterize these channel bodies, representative stratigraphic sections were logged, and the orientations of bounding surfaces and palaeocurrent indicators were measured (330 measurements, 318 of which correspond to different types of cross-bedding). A record of the orientation of the channel bodies was hampered by the overall limited three-dimensionality of the outcrops, but the likely orientation of the channel bodies could nevertheless be inferred in the field thanks to the presence of additional palaeocurrent indicators (imbricated clasts, sole marks) and the orientation of cut-banks that are locally exposed in three dimensions. A total of 257 logs were measured (516 m cumulative thickness); they record information from 180 channel bodies. Additionally, for an overall characterization of the entire succession, 15 continuous stratigraphic logs (882 m cumulative thickness) were measured using a Jacob staff with a laser sighting stage designed for precise thickness measurement (Patacci, 2016). In addition to the detailed sedimentological and stratigraphic work in the Arén-Esplugafreda sector, observations of the Upper Red Garumnian near the localities of Claret and Gurp (Fig. 1C) were also gathered. For sedimentological logging, the lithofacies scheme of Colombera et al. (2013), itself a modified version of the fluvial lithofacies scheme by Miall (1996), was used. For the description and interpretation of bounding surfaces, the scheme of Tedesco et al. (2010), which is based on the classic scheme of Miall (1996), was used. To describe the geometry and shape of channelized elements based on their width-to-thickness ratio, the nomenclature of Gibling (2006) was adopted. In the case of conglomeratic bodies coarser than granulestone, the modal clast size was determined by the count of 20 gravel fragments; the size of the single largest clast, following the methodology of Lindholm (1987), was also determined. For the grain-size description of gravel fractions, the Udden-Wenthworth modified scale of Blair and McPherson (1999) was used.

4. Local geology of the Upper Red Garumnian

Based on the integration of the photogeological interpretation with the field study, the Upper Red Garumnian in the study area has been subdivided in four intervals (1 to 4 from base to top). Mapping results of these four intervals and of the different types of conglomerate and sandstone bodies (channelized elements and sediment gravity-flow deposits) are shown in Figs. 3 and 4 for the Arén and Esplugafreda areas, respectively. Rose diagrams with the restored palaeocurrent (cross-stratification and cross-lamination) data are shown for each area. Palaeocurrent vector means consistently indicate a SSE to SSW sediment-transport direction, in agreement with the notion of the outcrop belt being oriented approximately along strike; however, important dispersion in palaeocurrent orientations is seen, which is compatible with the interpretation of a relatively low-gradient fluvial plain. The basal boundary of interval 1 is not exposed. The basal boundary of the intervals 2–3 has been defined in local stratigraphic sections and laterally extrapolated thanks to the consistent stratigraphic occurrence of basal coarse-grained conglomeratic deposits or correlative unconfined heterolithic deposits. However, there are extensive sectors where these coarser-grained deposits are absent, and the corresponding boundary cannot be traced confidently. The basal boundary of the Interval 4 corresponds locally to the Claret Conglomerate, which can be readily identified in outcrop, or to the base of underlying localised valley fills. Representative lithofacies are shown in Fig. 5. Vertical profiles recording successions of these lithofacies for the Arén (Fig. 6) and Esplugafreda

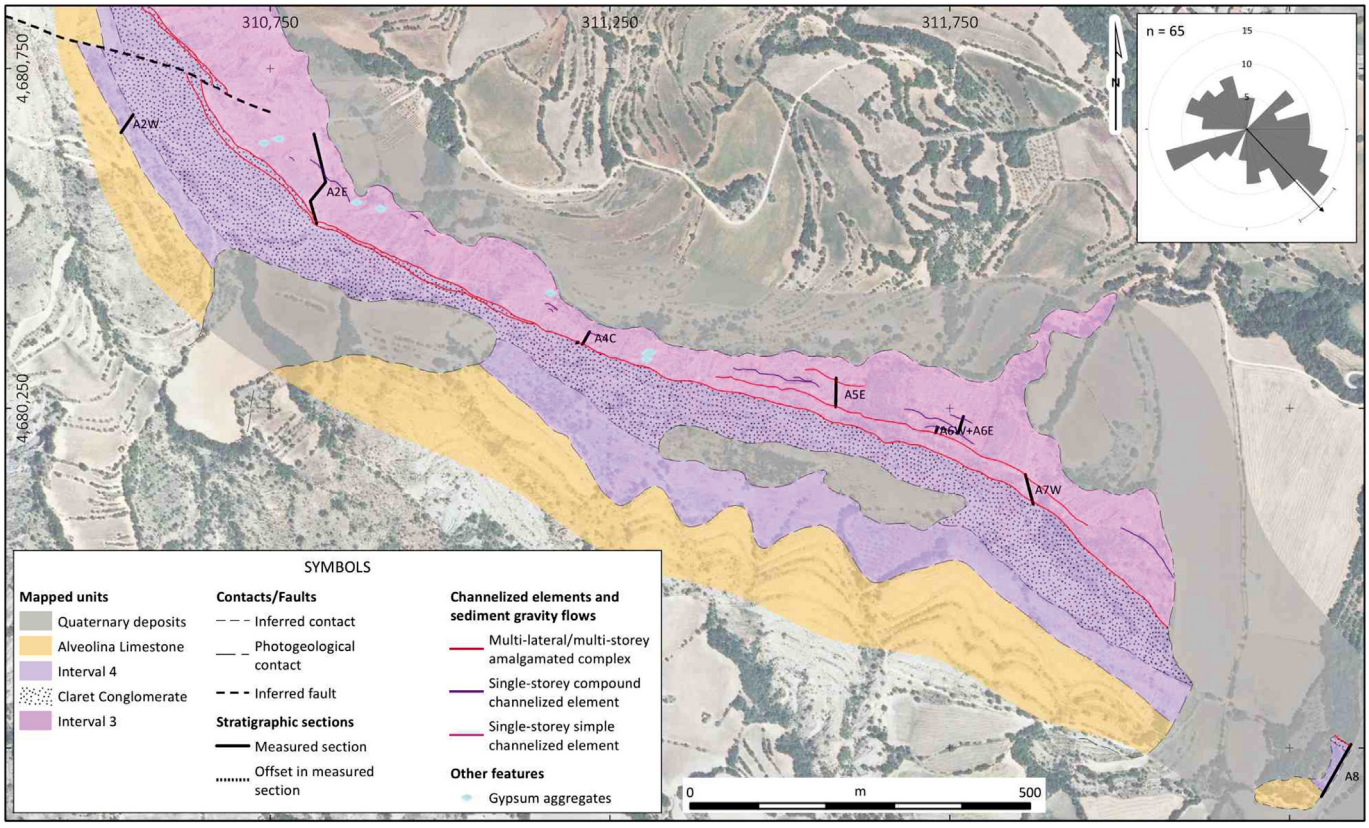

Fig. 3. Detailed geological map of the Arén sector showing the mapped channelized elements (traces of surfaces delineating bases and lateral margins) along with concentrations of gypsum precipitates and the measured stratigraphic logs (A2W to A8). Palaeocurrent data show a wide dispersion with a vector mean to SE. The Claret Conglomerate has a significant planform extent because it tends to form a slope. See Fig. 1 for location.

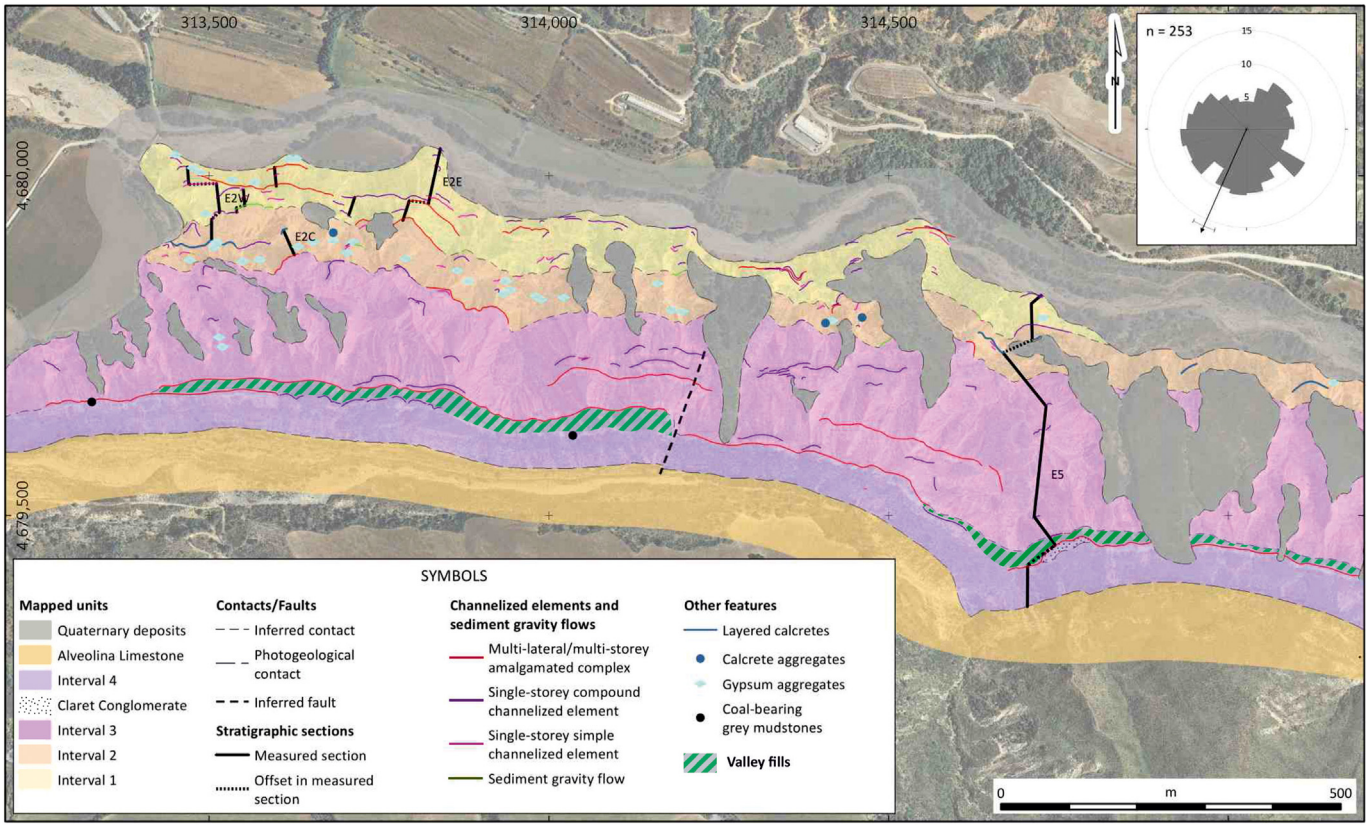

Fig. 4. Detailed geological map of the westernmost part of the Esplugafreda sector showing the mapped channelized elements and sediment gravity flow deposits (traces of surfaces delineating bases and lateral margins), along with pedogenic carbonates, gypsum precipitates, occurrences of coaly mudstones and the measured stratigraphic logs (E2W to E5). Palaeocurrent data show high dispersion with a mean vector toward SSW. See Fig. 1 for location.

sections (Fig. 7) highlight the predominance of fine-grained lithofacies in the Upper Red Garumnian.

5. Lithofacies

Fourteen lithofacies were identified, principally on the basis of their texture and sedimentary structures (Table 1; Fig. 5). These lithofacies comprise conglomerates (four types), sandstones (six types), fine-grained lithofacies (three types) and pedogenic carbonates. The fine-grained lithofacies comprise (i) massive packages of mudstones and siltstones (Fsm lithofacies) and (ii) interbeds of very fine-grained sandstones and siltstones (Fl lithofacies). For each of these fine-grained lithofacies, two subtypes have been defined, based on colour variations from red to grey hues, and respectively designated by addition of *r* (red) and *g* (grey) letters after the main lithofacies code. The third fine-grained lithofacies (Fmc), which shows a very restricted stratigraphic occurrence, consists of grey-coloured mudstones with coaly fragments. Concentrations of pedogenic calcareous nodules (P lithofacies) form a distinct, non-clastic lithotype. The detrital components of the conglomeratic and arenaceous lithofacies described here are usually calciclastic sensu Braunstein (1961).

6. Depositional and architectural elements

The Upper Red Garumnian succession in the studied area comprises three main depositional elements associated with specific sedimentary processes and settings: (i) *channelized fluvial deposits*, (ii) *sediment gravity-flow deposits* and (iii) *fluvial non-channelized deposits*. In these types of depositional elements, six classes of architectural elements have been defined. Channelized deposits comprise three architectural-element types, which are distinguished according to their geometry and degree of complexity defined by their internal architecture. Sediment gravity-flow deposits are represented by a unique element type. Non-channelized deposits are represented by two types of elements defined according to their geometry, dominant lithotypes and interpreted relative distance away from genetically related fluvial channel deposits. Representative sketches and logs of these six types of architectural elements, together with pie charts depicting overall proportions of lithofacies in each type based on cumulative facies thickness, are shown in Fig. 8. Statistics referring to the thickness, apparent width and width-to-thickness (W/T) ratios of the coarse-grained bodies (channelized elements and sediment gravity flow deposits) are shown in Table 2.

6.1. Channelized fluvial deposits

The subdivision here established for channelized deposits comprises three different types: (i) simple single-storey channelized elements (FC1); (ii) compound single-storey channelized elements (FC2); and (iii) multi-storey and multilateral channelized elements (FC3). The distinction between these different elements is based on their preserved geometry, internal architecture, and recognition and interpretation of the bounding surfaces delimiting these bodies and their constituent packages of strata. Simpler channelized bodies (FC1 and FC2) record mostly vertical aggradation processes, whereas more complex bodies (FC3) show more diverse architectural styles, including evidence of lateral and downstream barform accretion. However, it is important to note that because the orientation of the Arén and Esplugafreda outcropping sections is mostly normal to slightly oblique with respect to the dominant palaeoflow direction, downstream accretion geometries may be underrecognized in the available exposures.

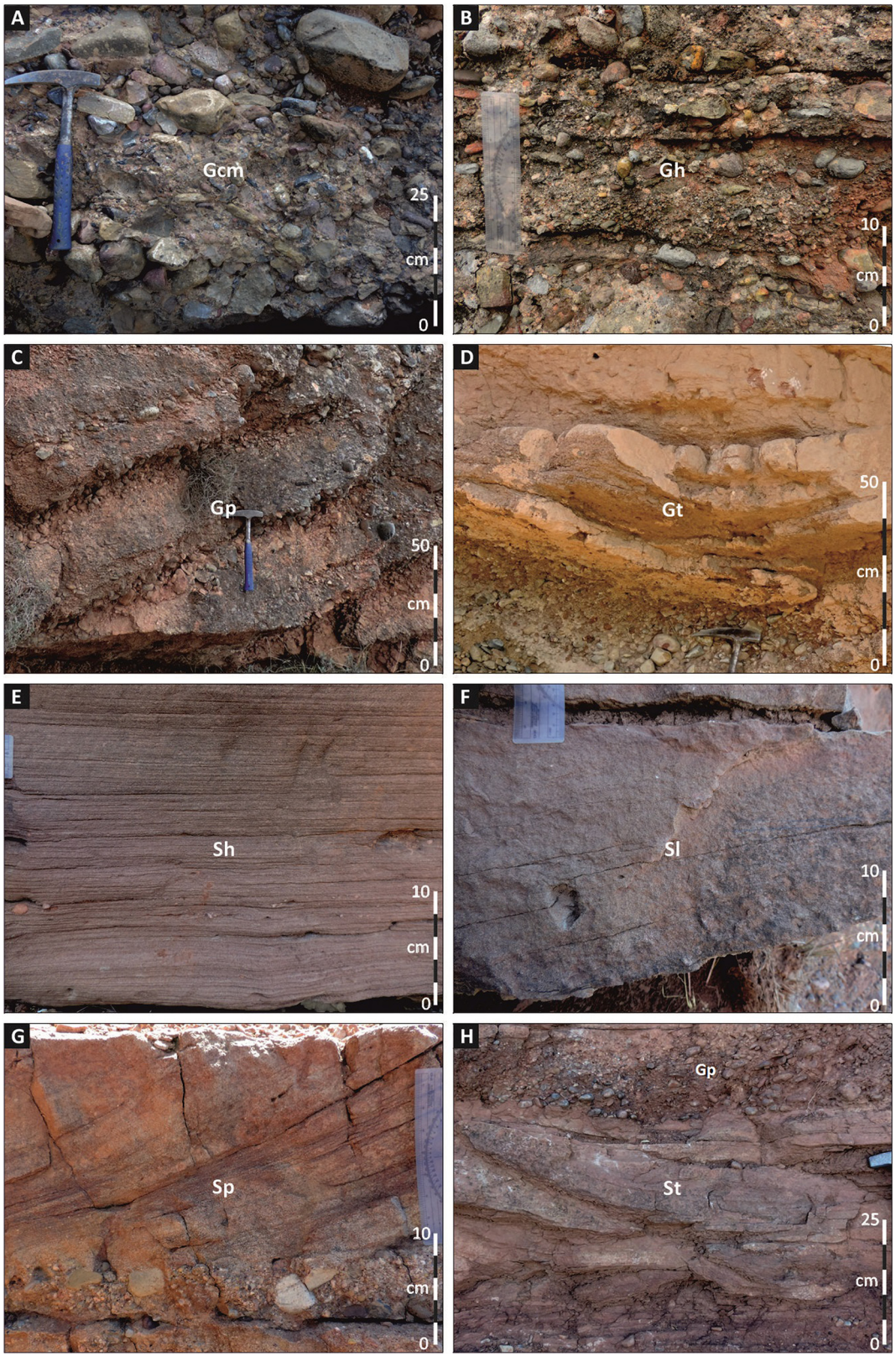

Fig. 5. Lithofacies defined in the 'Upper Red Garumnian'. A. Massive conglomerates (Gcm); B. Conglomerates with horizontal bedding (Gh); C. Conglomerates with planar cross-bedding (Gp); D. Conglomerates with trough cross-bedding (Gt); E. Sandstones with horizontal bedding (Sh); F. Sandstones with low-angle cross-bedding (Sl); G. Sandstones with planar cross-bedding (Sp); H. Sandstones with trough cross-bedding (St).
I. Massive conglomeratic sandstones (Sm); J. Sandstones with ripple-bedding (Sr); K. Interbeds of red-coloured siltstones and very fine-grained sandstones (Flr); L. Interbeds of grey-coloured siltstones and very fine-grained sandstones (Flg); M. Red-coloured massive mudstones to siltstones (Fmr); N. Grey-coloured massive mudstones to siltstones (Fsmg); O. Grey coloured mudrocks with coaly streaks and fragments (Fmc); P. Light-coloured pedogenic carbonates with massive to nodular structure (P).

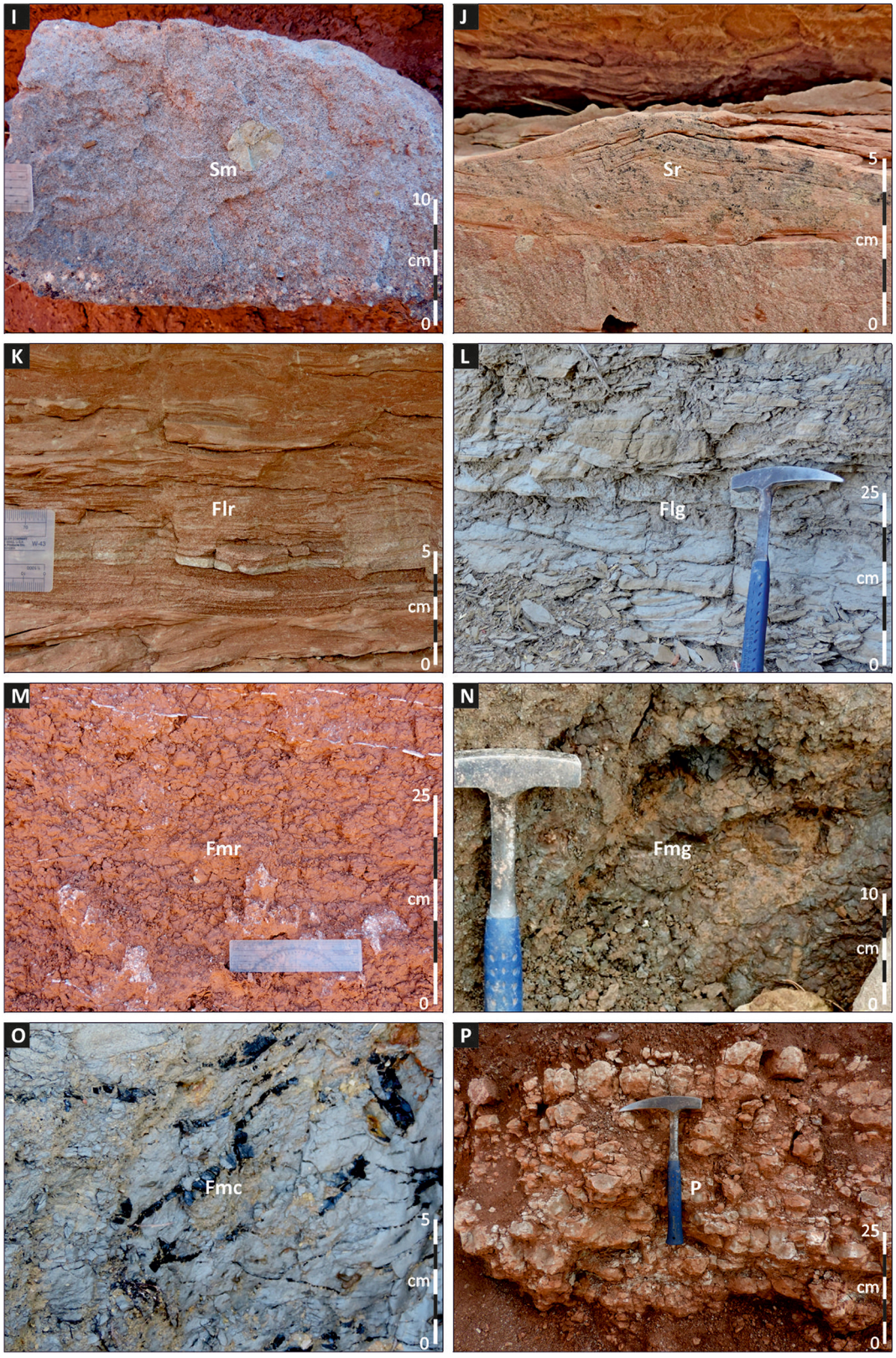

Fig. 5 (*continued*).

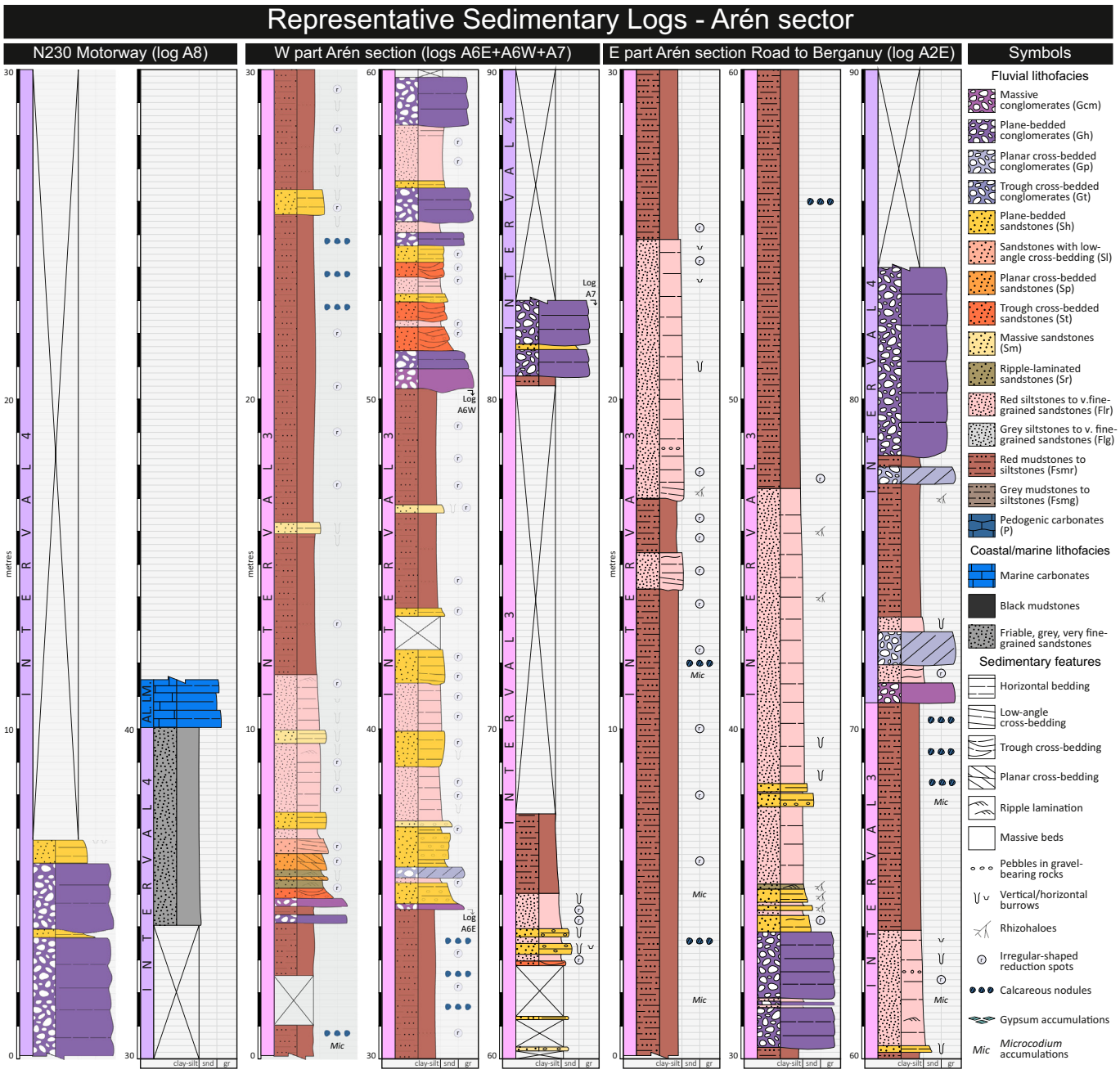

Fig. 6. Representative logs from the Arén section. See Fig. 3 for the location of the logs. Log A8 is from the vicinity of the 100 km marker of the N230 motorway.

6.1.1. Simple single-storey channelized elements (FC1)

6.1.1.1. Description. Thirty-nine instances of these channelized elements were described and recognized in all the stratigraphic intervals defined for the Upper Red Garumnian in the study area; they tend to be more common in the intervals 1 and 2. The thickness of these elements ranges from 0.5 m to 1.3 m; their average apparent width is 11.8 m. According to their apparent width-to-thickness ratios, they mostly comprise of broad ribbons to narrow sheet-like bodies (Table 2). The base of these elements is sharp and corresponds to 4th-order bounding surfaces (Miall, 1985), whose relief is mostly flat or slightly concave-upward (Fig. 9A), and only locally irregular and strongly incisional. These elements are outlined by a single channel form, here termed as 'storey'.

In most cases (26 examples), these elements are dominated internally by either conglomeratic or sandy facies, with no marked grainsize trend (Fig. 9B); in 12 cases, a fining-upward trend is observed, usually associated with the vertical superposition of sandstone lithofacies above a basal conglomerate; only one example of coarsening-upward pattern was documented. Horizontally bedded conglomerates (Gh: 39.66%) and sandstones (Sh: 26.1%) are the dominant lithofacies. Conglomerates and sandstones with planar cross-bedding are observed in lower proportions (Gp: 11.2% and Sp: 10.7% respectively), and can either occur indistinctly as the only lithofacies present, or be preferentially located at the base (Fig. 9C) or toward the top (Fig. 9D) of these channelized elements; massive conglomerates (Gcm) attain an abundance of 6.4%; other lithofacies types occur in percentages lower than 5%; only one example of rippled-sandstones capping the channel fill was recorded; fine-grained (F lithofacies) are not observed in these channel bodies.

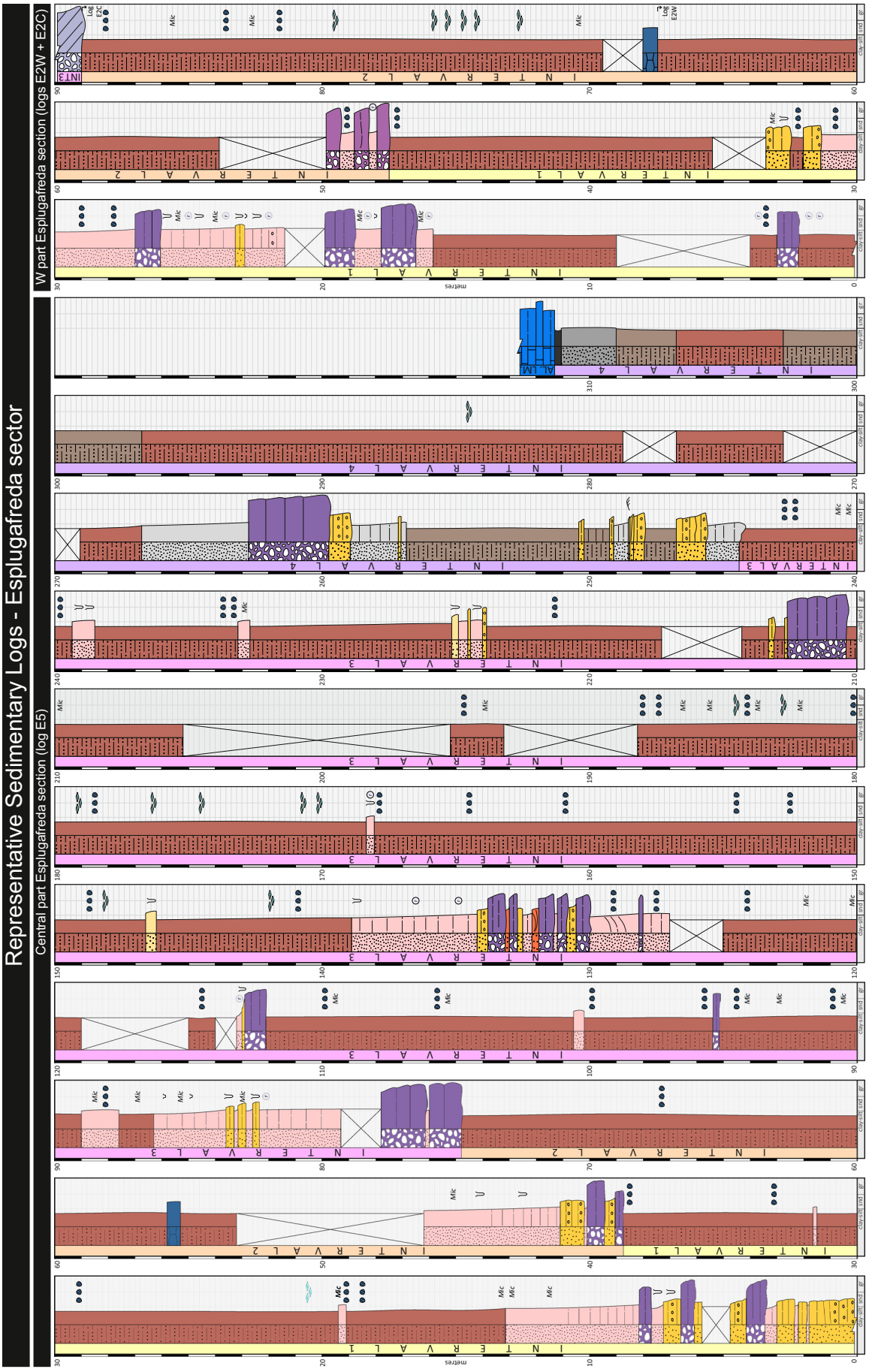

Fig. 7. Representative logs from the Esplugafreda section. See Fig. 4 for the location of the logs and Fig. 6 for key of facies and other sedimentary features.

Table 1
Summary of lithofacies observed in the 'Upper Red Garumnian' in the Arén-Esplugafreda sector.

Facies Code	Grain size	Sedimentary structures	Biogenic/pedogenic features	Interpretation
Gcm	Very poorly to poorly sorted, clast-supported, medium-pebble to fine-cobble conglomerates	Massive beds	None recorded	High flow stage deposition by streamflows (Hassan et al., 2009) or non-cohesive sediment-gravity flows (Went, 2005; Blair and McPherson, 2009)
Gh	Poorly to moderately sorted, fine- to very coarse-pebble conglomerates	Horizontal stratification in medium to coarse beds (0.1–1 m)	Infrequent occurrence of basal horizontal burrows (finer-grained varieties)	High-energy deposition associated with gravel sheets migration in streamflows (Hassan, 2005; Hassan et al., 2009)
Gt	Poorly to moderately sorted, granule to very coarse-pebble conglomerates	Trough cross-bedding in coarse beds (0.3 m–1 m)	None recorded	Downstream migration of three-dimensional dunes and bars or fill of minor depressions located in the deeper parts of channels (Miall, 1978)
Gp	Poorly to moderately sorted, granule to very coarse-pebble conglomerates	Planar cross-bedding in medium to very coarse beds (0.1–3 m)	None recorded	Downstream migration of bars or straight-crested dunes in the deeper parts of channels (Miall, 1978)
Sh	Poorly to well-sorted, occasionally conglomeratic, very fine- to very coarse-grained, sandstones	Planar horizontal bedding, with occasional current parting lineation; grading (normal and inverse) in conglomeratic varieties	Burrows, rhizohaloes and irregular drab haloes; occasional *Microcodium*, especially in finer-grained varieties	High-velocity shallow flows under upper flow-regime conditions (McKee et al., 1967; Williams, 1971; Tunbridge, 1981; Parkash et al., 1983)
Sl	Moderately to well-sorted, fine- to coarse-grained sandstones	Low-angle cross-bedding (<10°). Laterally and vertically associated with Sh facies	Burrows, rhizohaloes and irregular drab-haloes	High-velocity flow into low-relief scours or migration of low-relief bedforms (Fielding, 2006)
Sp	Moderately to well-sorted, occasionally conglomeratic, fine- to coarse-grained sandstones	Planar cross-bedding in medium to coarse beds (0.1 m–1 m)	Uncommon burrows and irregular drab-haloes in finer grained varieties	Downstream migration of two-dimensional dunes under lower flow-regime (Parkash et al., 1983; Abdullatif, 1989)
St	Moderately to well-sorted, occasionally conglomeratic, fine- to coarse-grained sandstones	Trough cross-bedding in medium to coarse beds (0.1–0.6 m)	Rare rhizohaloes and irregular drab haloes in finer grained varieties	Downstream migration of three-dimensional dunes under lower flow-regime (McKee et al., 1967; Williams, 1971; Parkash et al., 1983)
Sm	Poorly sorted, fine to very coarse-grained, occasionally conglomeratic, sandstones	Massive beds, with uncommon grading (normal and inverse) in conglomeratic varieties	Common burrows, rhizohaloes and irregular drab-haloes	Rapid deposition associated with highly concentrated sediment load (Fisher et al., 2008); the massive structure may also be a product of biogenic activity (Miall, 1996)
Sr	Well-sorted, very fine- to fine-grained sandstones	Ripple cross-lamination, wavy bedding, small-scale cross-bedding	Uncommon rhizohaloes and irregular drab-haloes	Deposition under waning lower flow-regime by migration of current ripples (McKee et al., 1967; Tunbridge, 1981; Abdullatif, 1989)
Flr and Flg	Interbeds of siltstones with very fine-grained sandstones (Flr: red-coloured; Flg: grey-coloured)	Horizontal lamination, ripple bedding, synsedimentary deformation structures. Usually massive because of bio/pedoturbation	Abundant burrows, rhizohaloes and irregular drab haloes and *Microcodium* accumulations; occasional leaf imprints	Waning channelized flows and unconfined, decelerating, shallow flows (Hubert and Hyde, 1982; Wells, 1983; Sadler and Kelly, 1993).
Fsmr and Fsmg	Mudstones to siltstones (Fsmr: red-coloured; Fsmg: grey-coloured)	Mainly massive beds, only with occasional relicts of horizontal lamination	Mottling, occasional burrows and irregular drab haloes and *Microcodium* accumulations	Suspension settling deposition in relation to unconfined floods (Parkash et al., 1983; Stear, 1983; Wells, 1983; Cowan, 1993)
Fmc	Grey-coloured mudstones with coaly fragments	Relicts of lamination defined by coaly streaks	Centimetric coaly fragments and streaks	Suspension settling deposition related to ponded areas with reducing conditions, but high supply of suspended-sediment load (Takano and Waseda, 2003)
P	Pedogenic carbonates	Massive or with faint nodular structure	Locally associated with rhizoconcretions	Product of carbonate precipitation in floodplains in relation to negative water balance in soils (Reineck and Singh, 1980), or in a palustrine setting (Alonso-Zarza and Wright, 2010)

6.1.1.2. Interpretation. These bodies are interpreted to record the infill of a channel form associated with the development of bedload sheets or dunes. Bedding surfaces can be associated with minor changes in flow conditions. Channel bodies dominated by plane-bedded conglomeratic and arenaceous lithofacies can result from bedload deposition associated with shallow and high-energy floods, formed under upper flow-regime conditions (Williams, 1971; Wells, 1983; Abdullatif, 1989; Hassan et al., 2009; Reid and Frostick, 2011). Cross-bedded facies can be associated with flows having a deeper water column and lower flow-regime conditions (Fielding, 2006). The limited occurrence of sandstone with ripple lamination in similar ancient deposits has been associated with rapidly waning flows (Tunbridge, 1984). The single-storey nature of these channel bodies and the general absence of fine-grained partings suggest, in most cases, deposition from a single flood event (Tunbridge, 1981). The occurrence of massive conglomerates as basal channel-fill deposits can be associated with gravel accumulations related to gravel bars, as seen in recent ephemeral streams (Hassan, 2005), which are deposited during high flow stages (Hassan et al., 2009).

6.1.2. Compound single-storey channelized elements (FC2)

6.1.2.1. Description. Among the coarse-grained bodies described in the Upper Red Garumnian, these elements are the most abundant with 108 examples recorded; they occur indistinctly in the four intervals defined. Their maximum thickness ranges from 0.8 m to 5.6 m, but most of the bodies show values between 1.0 m and 2.9 m; their average apparent width is 26.1 m. The apparent width-to-thickness ratio indicates approximately equal occurrence of broad or narrow ribbon bodies and narrow sheet-like bodies (Table 2). The basal surfaces of these elements, corresponding to 5th-order bounding surfaces, can be planar (Fig. 10A), else concave-upward and very irregular (Fig. 10B and C). Where observed, the margins are incisional and can be very steep (Fig. 10A).

Internally, FC2 elements are single-storey but composed of vertically stacked strata sets separated by 3rd-order surfaces. These surfaces show a planar to moderately concave-upward relief. Due to the occurrence of multiple internal sets, the overall grain-size pattern of these channel bodies is highly variable; some elements can display a fining-upward trend (Fig. 10A), whereas others are capped by conglomeratic

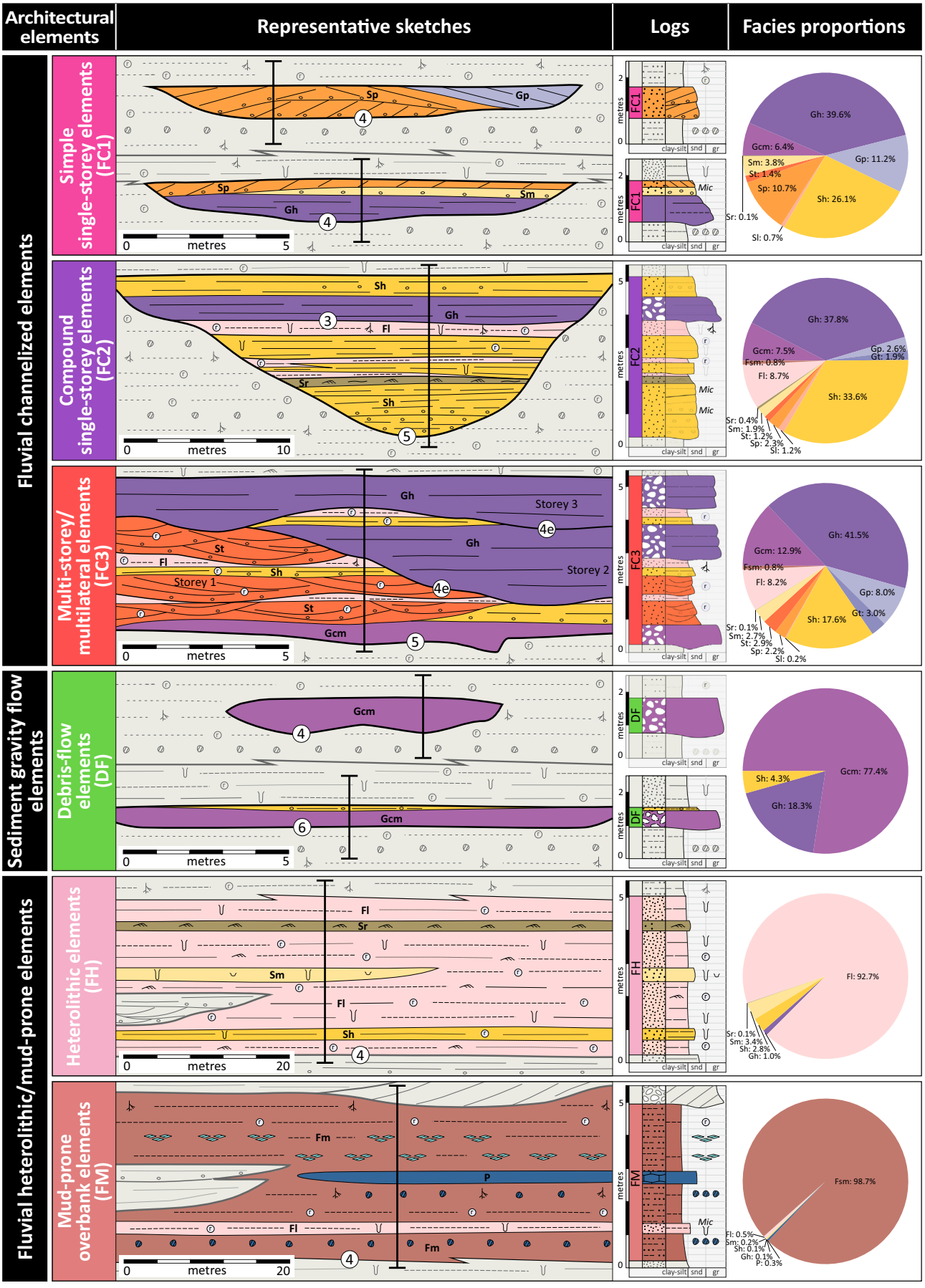
Architectural elements
Representative sketches
Logs
Facies proportions
Fluvial channelized elements
Simple single-storey elements (FC1)
Compound single-storey elements (FC2)
Multi-storey/ multilateral elements (FC3)
Sediment gravity flow elements
Debris-flow elements (DF)
Fluvial heterolithic/mud-prone elements
Heterolithic elements (FH)
Mud-prone overbank elements (FM)
Sp
Gp
Sm
Gh
Sh
Fl
Sr
St
Gcm
Fm
P
Storey 1
Storey 2
Storey 3
4e
0 metres 5
0 metres 10
0 metres 20
metres
clay-silt snd gr
Mic
Gh: 39.6%
Gcm: 6.4%
Gp: 11.2%
Sm: 3.8%
St: 1.4%
Sp: 10.7%
Sh: 26.1%
Sr: 0.1%
Sl: 0.7%
Gh: 37.8%
Gcm: 7.5%
Gp: 2.6%
Gt: 1.9%
Fsm: 0.8%
Fl: 8.7%
Sh: 33.6%
Sr: 0.4%
Sm: 1.9%
St: 1.2%
Sp: 2.3%
Sl: 1.2%
Gh: 41.5%
Gcm: 12.9%
Fsm: 0.8%
Fl: 8.2%
Gp: 8.0%
Gt: 3.0%
Sh: 17.6%
Sr: 0.1%
Sm: 2.7%
St: 2.9%
Sp: 2.2%
Sl: 0.2%
Gcm: 77.4%
Sh: 4.3%
Gh: 18.3%
Fl: 92.7%
Sr: 0.1%
Sm: 3.4%
Sh: 2.8%
Gh: 1.0%
Fsm: 98.7%
Fl: 0.5%
Sm: 0.2%
Sh: 0.1%
Gh: 0.1%
P: 0.3%

lithofacies (Fig. 10B and D). In most cases, each bedset shows internally a decrease in grain size, with lower beds of conglomerates and sandstones overlain by fine-grained lithofacies (see the different examples in Fig. 10). As in the previous case, horizontally bedded conglomerates and sandstones are the most abundant lithofacies, with respective values of 37.8% and 33.6%; massive conglomerates (Gcm: 7.5%) and fine-grained heterolithic lithofacies (Fl: 8.7%) are also notable; other lithofacies, including cross-bedded conglomerates and sandstones, occur in percentages lower than 3%. Some of the sandstone lithofacies rarely show intense bioturbation, although this is more common in the fine-grained lithofacies, which additionally show the development of mud-cracks.

6.1.2.2. Interpretation. These bodies are interpreted to record a channel-filling process associated with the vertical stacking of the deposits of bedload sheets, upper flow regime plane-beds and, subordinately, 2D and 3D dunes. They record different flow conditions occurring in the same fluvial channel; the product of individual flows are usually separated by mud-drapes, which formed during waning stages; the very limited degree of scouring indicates that limited erosion took place between and during different flow events (cf. Picard and High, 1973; Hampton and Horton, 2007).

6.1.3. Multi-storey and multilateral channelized elements (FC3)

6.1.3.1. Description. Twenty-five examples of the studied channel bodies correspond to multi-storey and/or multilateral channelized elements (FC3); these are present in all the four stratigraphic intervals defined for the Upper Red Garumnian in the studied area. The maximum thickness of these channel bodies is variable and ranges from 2.1 to 9.4 m; their average apparent width is 246.9 m. Their overall geometry, defined by their apparent width-to-thickness ratio, indicates the predominance of narrow and broad sheet-like bodies over ribbon-shaped bodies (Table 2). The basal surface of these elements can correspond to planar 5th-order, or, in some cases (e.g. the Claret Conglomerate), 6th-order surfaces delimiting major and laterally continuous stratigraphic packages (Fig. 11A). An upward increase in the apparent width of these elements is observed, specifically in the uppermost part of the interval 3 (maps of Figs. 3 and 4), and reaching a more significant expression in the Claret Conglomerate, where bodies attain apparent widths of more than 700 m.

The internal geometry of these elements indicates the vertical, lateral and downstream superposition (stacking) of macroforms separated by 4th-order surfaces, which are either erosional (4e, Figs. 11A, B and C) or accretionary (4a, Fig. 11A and D) in nature; erosional reactivation surfaces can show prominent (metric) relief, with evident excavation of the older coarse-grained deposits (Fig. 11B and C); accretionary surfaces can display moderate relief in oblique to strike views (Fig. 11A), but in other cases can correspond to the steep lee face of conglomeratic bars onlapped by channel fill deposits (Fig. 11D). Individual macroforms are between 1 m and 4 m thick, and comprise mostly coarse-grained associations of conglomerates and sandstones; rarely finer-grained fills of mudrocks and fine-grained sandstones are also present (Fig. 11D). As in the previous examples of channelized elements, horizontally bedded conglomerates (Gh: 41.5%) and sandstones (Sh: 17.6%) are the dominant lithofacies; in addition, massive conglomerates can be abundant (Gcm: 12.9%) and may occur in association with planar cross-bedded conglomerates (8.0%); heterolithic siltstones and fine-grained sandstones also represent an important component (8.2%); other lithofacies types are subordinate and occur with percentages of less than 3.0%. Subordinate finer-grained lithofacies (Fsm and Fmc, less than 1%) exhibit pedoturbation, in the form of reddish mudstone with calcareous nodules, rhizoliths and mudcracks, or occur as localized lenses of grey mudstone with coaly fragments (restricted to interval 4). The occurrence of oncoidal coatings around some gravel-sized clasts in conglomeratic beds is restricted to some channelized elements of the interval 4, specifically of the Claret Conglomerate.

Table 2
Statistical summary of dimensional data of channelized elements and sediment-gravity-flow elements. Min. = minimum; Max. = maximum; Std. dev. = standard deviation. N denotes the number of channelized elements.

	N	Min.	Max.	Mean	Std. dev.
All sedimentary-body types					
Thickness (m)	180	0.5	9.4	2.3	1.5
Apparent width (m)	180	2.5	985.7	53.1	131.2
Width-to-thickness ratio	180	1.5	281.5	19.6	31.5
Simple single-storey channelized element (FC1)					
Thickness (m)	39	0.5	1.3	0.8	0.2
Apparent width (m)	39	2.5	49.9	11.8	10.3
Width-to-thickness ratio	39	4.2	52.5	14.9	11.5
Compound single-storey channelized element (FC2)					
Thickness (m)	108	0.8	5.6	2.5	1.2
Apparent width (m)	108	3.7	129.3	26.1	24.5
Width-to-thickness ratio	108	1.5	75.3	12.0	11.0
Multi-storey/multilateral channelized elements (FC3)					
Thickness (m)	25	2.1	9.4	4.1	1.7
Apparent width (m)	25	11.9	985.7	246.9	278.0
Width-to-thickness ratio	25	3.6	281.5	61.2	66.1
Debris-flow deposits (DF)					
Thickness (m)	8	0.5	1.3	1.0	0.3
Apparent width (m)	8	4.8	29.2	12.3	7.7
Width-to-thickness ratio	8	4.3	31.4	14.0	9.8

6.1.3.2. Interpretation. These multi-storey and multilateral channelized elements are inferred to represent deposition in active fluvial channel belts (cf. Gibling, 2006). Predominance of plane-bedded conglomerates over massive conglomerates indicates prevalence of bedload sedimentation by high-energy flows (Hassan, 2005; Hassan et al., 2009). The development of these multilateral and multistorey complexes suggests important channel mobility, possibly associated with repeated avulsions, driving the reworking of previous deposits (Hirst, 1991; Cain and Mountney, 2009). In most of the cases, especially in the lower part of the Upper Red Garumnian (intervals 1 and 2), these channelized elements present limited apparent widths, which indicates limited lateral displacement of the formative channel forms; internally, styles of vertical and, where recognizable, downstream growth are more evident, suggesting the recurrent occupation of the same channel. In contrast, more intensive lateral reworking and the occupation of more extensive floodplain areas (cf. North and Taylor, 1996) can be inferred for the upper part of the succession, from interval 3, and particularly in the Claret Conglomerate (interval 4). In the Claret Conglomerate, this change in architectural style has been interpreted as the response of the fluvial system to the PETM (Schmitz and Pujalte, 2007; Domingo et al., 2009; Colombera et al., 2017; Chen et al., 2018). Nonetheless, the gradual increase in the lateral extent of the FC3 elements observed in the interval 3 could imply a response of the fluvial system to allogenic factors that operated over a timescale longer than that of the PETM.

The local occurrence of oncolites in conglomeratic deposits of FC3 elements of the Claret Conglomerate can be associated with quiet-water conditions somewhere in the broader terrestrial environment, which allowed the growth of these coated grains in relation to microbial activity (Cojan, 1993; Arenas-Abad et al., 2010). In a similar way, the local occurrence of grey mudrocks with coaly fragments, suggest the development of ponded areas surrounded by vegetation, where organic

Fig. 8. Schematic 2D sketches, idealized logs, and pie charts of lithofacies proportions of the architectural elements defined in the Upper Red Garumnian, based on outcrop examples from the Arén and Esplugafreda sectors.

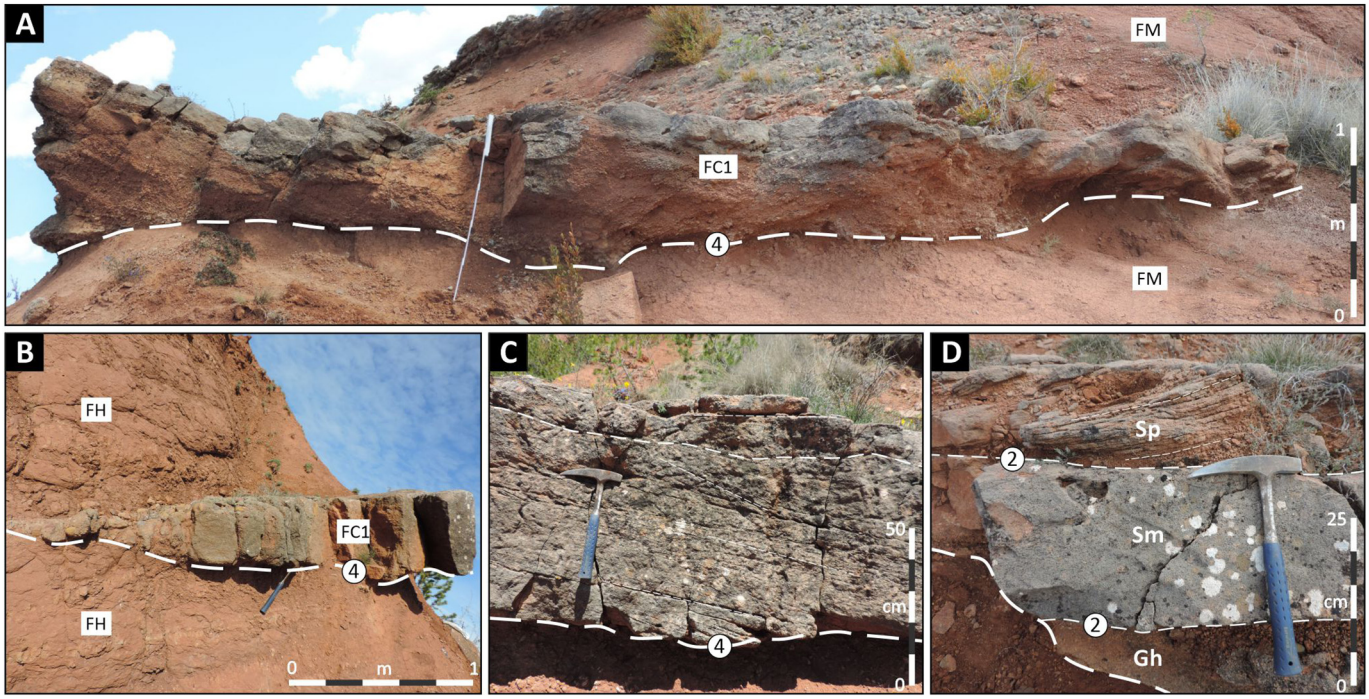

Fig. 9. Outcrop examples of simple single-storey channelized elements (FC1). A) Downdip view of a channel body (FC1; Esplugafreda sector - interval 1) encased within massive overbank deposits (FM); the channel body base corresponds to a slightly irregular concave-up 4th-order surface. B) Down dip view of the margin of a channelized element (FC1; Esplugafreda sector - interval 3) interposed between massive, highly bioturbated, unconfined heterolithic deposits (FH). C) Downdip view of a channelized element (Esplugafreda sector - interval 2) with a low-relief basal (4th-order) surface; internally this element comprises cross-bedded sandstones topped by low-angle to horizontally bedded sandstones. D) Detail of the simple single-storey channelized element shown in A, which comprises a fining-upward set of horizontal bedded conglomerates (Gh lithofacies) and massive to cross-bedded sandstones (Sm and Sp, respectively); these lithofacies are separated by 2nd-order bounding surfaces.

remains were preserved thanks to locally developed reducing conditions, but where peat accumulations could not form due to the high supply of terrigenous suspended load (Takano and Waseda, 2003).

6.2. Sediment gravity-flow deposits

These deposits are stratigraphically restricted and are represented by only one type of architectural element, consisting of mainly non-channelized coarse-grained bodies composed of disorganized, clast-supported conglomerates. In terms of lithofacies, these deposits can be locally similar to those of some channelized deposits, but they are coarser grained and more poorly sorted than similar massive conglomerates of streamflow origin.

6.2.1. Debris-flow deposits

6.2.1.1. Description. Only 8 bodies of this type were identified in the Upper Red Garumnian in the study area, and these are restricted to the interval 2, occurring dominantly in its basal part. Usually, these bodies appear at the base of fining-upward successions and are overlain by metre-thick intervals of unconfined heterolithic elements; locally, they also occur encased within overbank deposits (see below). The maximum thickness of these debris-flow deposits ranges from 0.5 m to 1.3 m. These deposits occur as non-channelized bodies, with tabular to lenticular shapes, which according to their width-to-thickness ratio mostly correspond to broad ribbons and narrow sheet-like bodies (Table 2). The lower boundary of these elements varies from planar (Fig. 12A) to irregular and erosional surfaces (Fig. 12B); such surfaces usually correspond to 5th-order bounding surfaces, but depending on their position in the succession, such lower boundaries can be ranked as 6th-order surfaces, which locally define the base of the interval 2 of the Upper Red Garumnian (Fig. 12A and C). The top surface is typically flat but can locally present a convex-upward shape (Fig. 12B).

Internally these deposits are notably homogeneous (Fig. 12A), but in some cases they can show a crude stratification by fabric defined by the alignment of discoidal clasts (Fig. 12B), or by grain size due to the occurrence of matrix-supported sectors of limited vertical (<0.3 m) and lateral (<2 m) extent (Fig. 12C). These deposits are mainly composed of mud-poor, clast-supported, massive conglomerates (Gcm; 77.4%); conglomerates with crude horizontal bedding (Gh: 18.3%) are also present; pebbly sandstones, also with horizontal bedding, occur more rarely (Sh: 4.3%).

6.2.1.2. Interpretation. These deposits, dominated by clast-supported, disorganized conglomerates, which are coarser grained compared to massive conglomerates of streamflow origin, represent the deposits of mass flows comparable in rheology with the non-cohesive sediment gravity (debris) flows described in numerous alluvial-fan environments (Blair and McPherson, 1994, 2009; Went, 2005). Although the occurrence of sediment gravity flows in fluvial environments is relatively uncommon (Blair and McPherson, 1994), deposits of debris flows interbedded with fluvial sediments are documented in systems from arid to semiarid climates (Graham, 1983; Jain et al., 2005; Horiuchi et al., 2009). Debris flows of this type can be formed by catastrophic discharge over loose colluvium and under arid conditions (Blair and McPherson, 2009). Available reconstructions locate the potential source areas for these deposits of the Upper Red Garumnian system at distances greater than 15 km (Capote et al., 2002; Arostegi et al., 2011). The availability of loose, coarse-grained material in these source areas, dominated by limestones and calcareous sandstones, and subject to a generally dry climate, can be postulated. A modern analogue to an alluvial catchment of this type, also dominated by limestones and influenced by a semiarid climate regime, has been described by Baker (1977). In accordance with their local palaeogeographic context, the bodies described here could represent the distal parts of extensive sheets of sediment gravity-flow deposits, reflecting their inherent

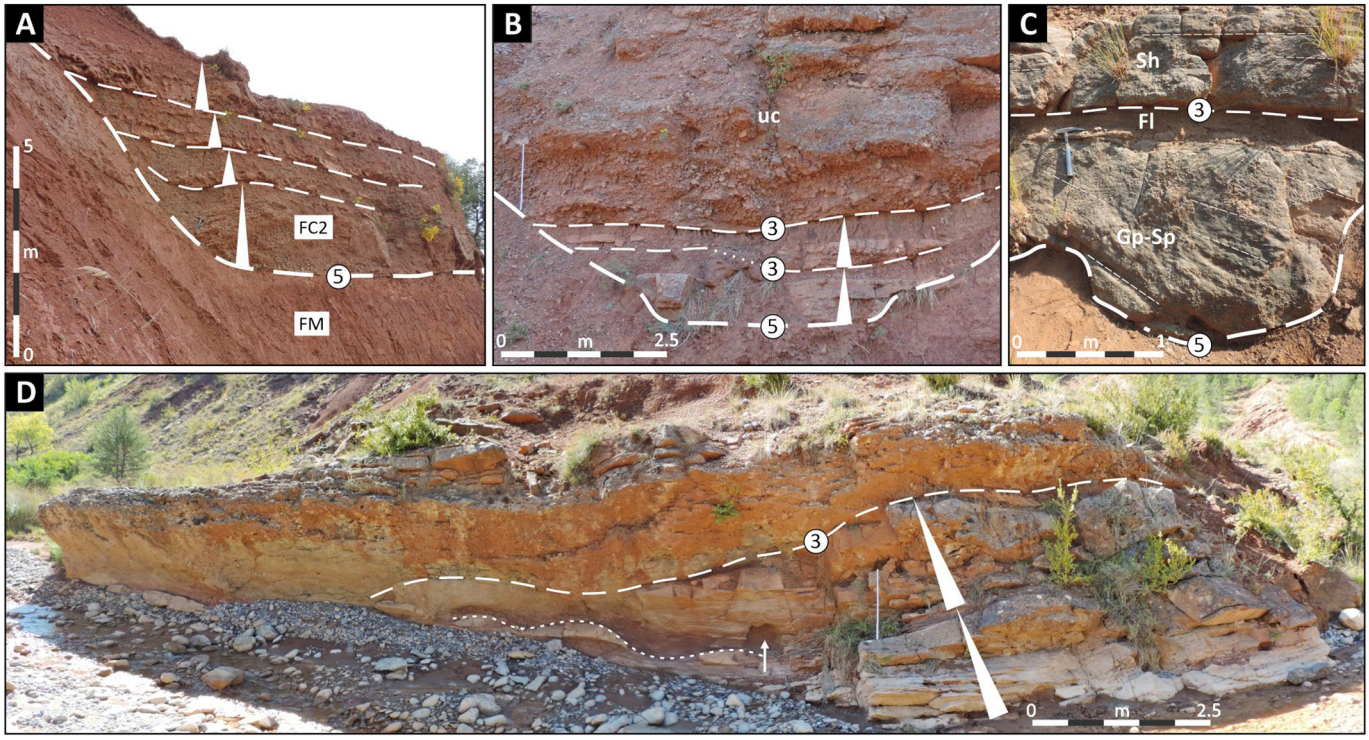

Fig. 10. Outcrop examples of compound single-storey channelized elements (FC2). A) Oblique view of the steep lateral margin and basal subhorizontal 5th-order bounding surface of a channel body (FC2) encased by massive overbank deposits (FM); the channelized element (Esplugafreda sector - interval 1) shows intense bioturbation and comprises of four different fining-upward sets (triangles) composed of conglomerates/sandstones and mudrocks. B) Strike view of a channel body (Arén sector - interval 3) with a concave-upward basal (5th-order) surface and internal low-relief 3rd-order surfaces bounding fining-upward lower couplets (triangles) and a thicker upper conglomeratic bedset (uc). C) Detail of a channelized element (Esplugafreda sector - interval 3) with a very irregular basal (5th-order) surface overlain by a fining-upward set consisting of cross-bedded conglomerates-sandstones (Gp-Sp lithofacies) capped by horizontal bedded sandstones and siltstones (Fl lithofacies); the topmost bed comprises sandstones with horizontal lamination (Sh lithofacies) deposited above a 3rd-order planar bounding surface. D) Oblique view of a channel body (Esplugafreda sector - interval 1) showing a lower fill composed of two fining-upward sets of sandstones and mudrocks (triangles); local convex-upward lenses of sandstone (lower line) and mud protrusion (arrow) reflect synsedimentary deformation; the upper part consists of conglomerates located above a low-relief 3rd-order bounding surface (upper line).

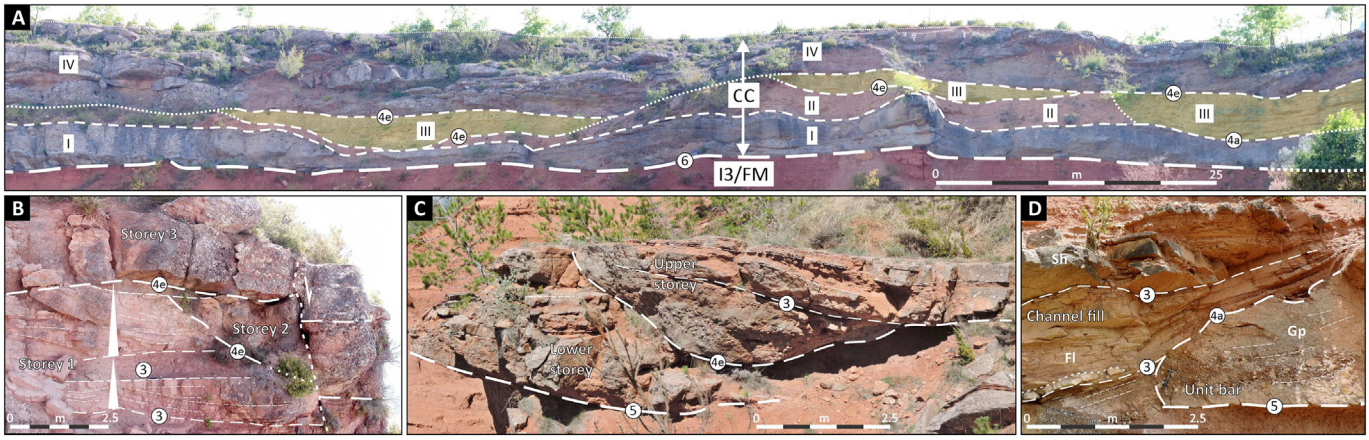

Fig. 11. Outcrop examples of multi-storey/multilateral amalgamated complexes (FC3). A) Oblique view of the Claret Conglomerate (CC) in the Arén sector (interval 4); this unit is bounded at the base by a low-relief 6th-order surface, which separates it from the underlying overbank deposits of the interval 3 (I3/FM). The CC comprises of different storeys separated by 4th-order accretionary (4a) and erosional (4e) surfaces: thick bedded, laterally amalgamated conglomeratic bodies (I and IV), laterally discontinuous interbeds of mudrocks and sandstones (II), and thinner-bedded conglomerates and sandstones within bodies with channelized geometry (III). B) Oblique view of a channelized element (Arén sector - interval 3) containing three different storeys; only the uppermost part of storey 1 is shown, and comprises two fining-upward sets of cross-bedded sandstones and mudrocks; storeys 2 and 3 are conglomeratic and their basal surfaces correspond to 4th-order erosional bounding surfaces with steep to planar relief. C) Downdip view of a channel body (Esplugafreda sector - interval 2) composed of two different storeys stacked in downstream direction; the surface separating such storeys corresponds to a 4th-order erosional surface (4e) with metric relief; in the lower storey the beds show horizontal bedding, whilst the upper storey displays downstream-accretion geometries. D) Detail of the contact between two different macroforms in an amalgamated complex (Esplugafreda sector - interval 1). The basal macroform corresponds to a unit bar deposited above a planar 5th-order surface and is composed of conglomerates with tangential cross-bedding (Gp lithofacies); the moderately steep lee face of this unit bar corresponds to a 4th-order accretionary bounding surface (4a), onlapped by strata of an aggradational channel-fill with interbeds of mudrocks and horizontally bedded sandstones (Fl and Sh lithofacies respectively); a lower sandstone bed within this channel fill shows a convex-up geometry (dotted line) and pinches out upslope, probably due to synsedimentary deformation related to deposition over an inclined surface.

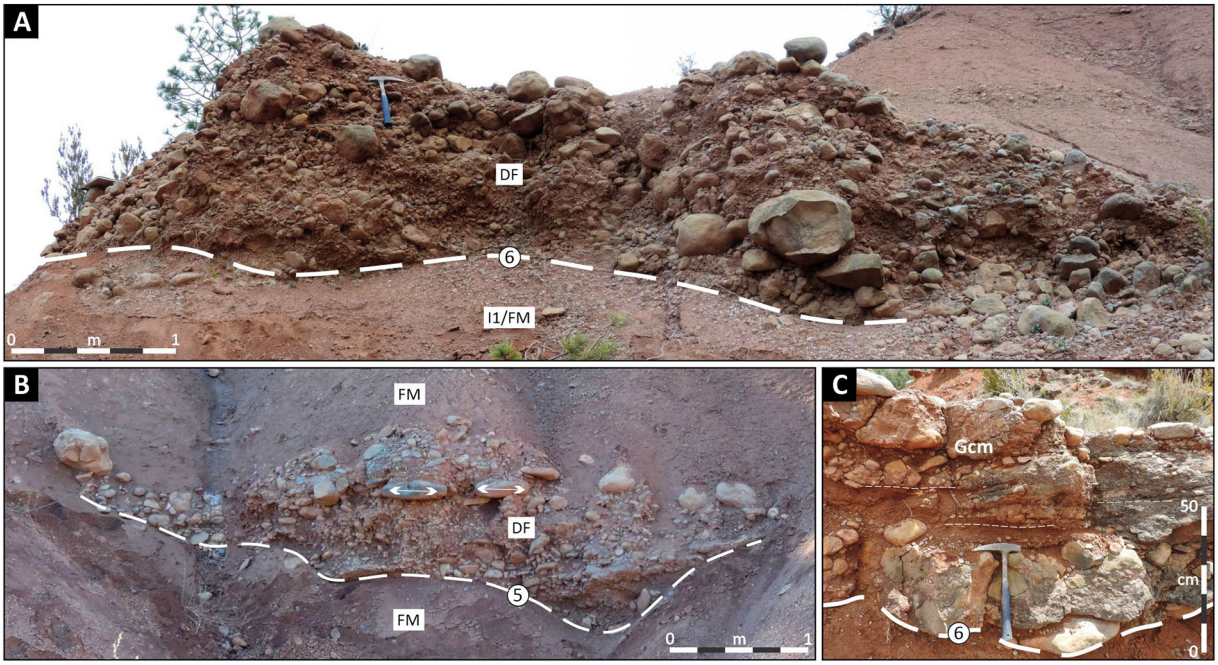

Fig. 12. Outcrop examples of debris-flow elements (DF). A) Oblique view of a debris flow element (DF) composed of disorganized, clast-supported conglomerate, with minor presence of muddy matrix surrounding fragments; the low-relief basal surface (6th-order) corresponds to the local boundary with the underlying interval 1 overbank deposits (I1/FM). B) Strike view of a debris-flow element (DF) encased within overbank deposits (FM); the DF element is composed of massive, mostly clast-supported conglomerates, locally with tabular fragments arranged horizontally (arrows); the lower 5th-order bounding surface is not sharp and shows an irregular concave-up geometry. C) Detail of a debris-flow deposit, mostly composed of clast-supported, massive conglomerates (Gcm lithofacies), but with a medial, laterally discontinuous, mud-supported sector associated with incipient horizontal bedding; as in A, the basal boundary corresponds to a 6th-order surface associated with the contact between intervals 1 and 2. All examples from the Esplugafreda sector (interval 2).

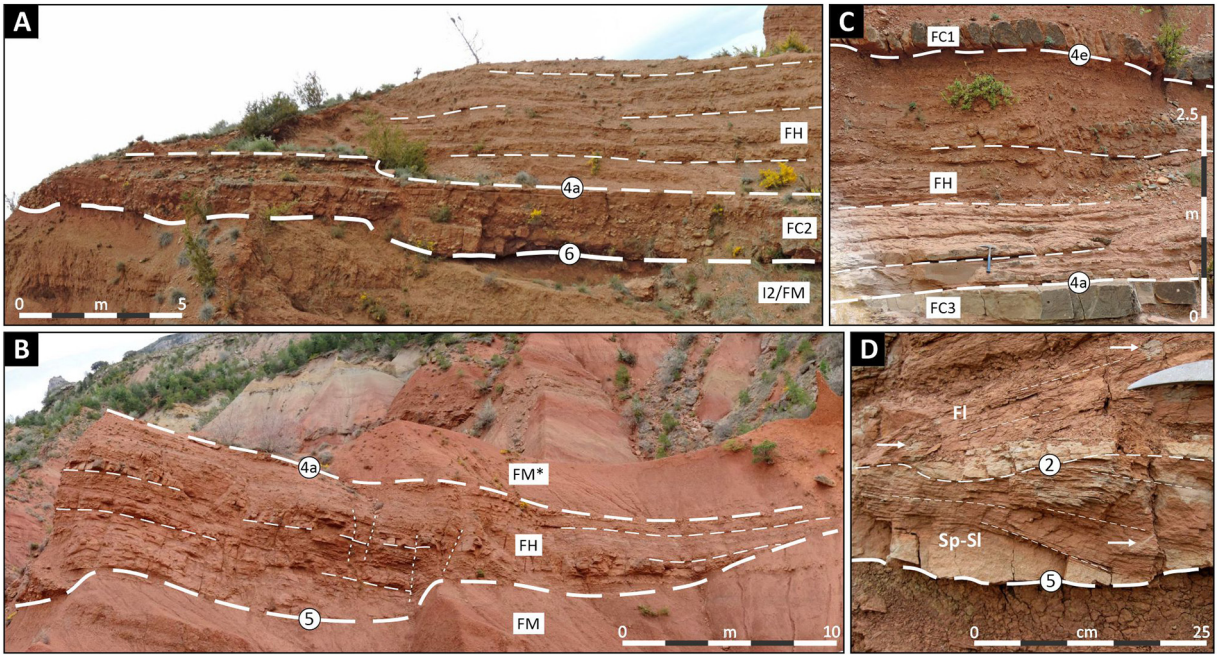

Fig. 13. Outcrop examples of unconfined heterolithic elements. A) Downdip view of an unconfined heterolithic element (FH, Esplugafreda sector - interval 3) located above a compound single-storey channelized element (FC2), which in turn overlies overbank deposits forming the topmost part of the interval 2 (I2/FM); lithological changes within the unconfined heterolithic element follow subhorizontal surfaces, which are diffuse due to intense biopedoturbation. B) Oblique view of the downslope end of an unconfined heterolithic element (FH, Esplugafreda sector - interval 3); the basal strata of these unconfined deposits onlap a slightly irregular relief (5th-order bounding surface), excavated into overbank deposits (FM); such relief may be locally controlled by minor normal faults (dotted sub-vertical lines); the upper contact (4a) instead is gradual with the overlying overbank deposits (FM*). C) Downdip view of an unconfined heterolithic element (FH, Esplugafreda sector - interval 1); the lowermost sandstone corresponds to the topmost bed of the overlying channelized element shown in 9D (FC3); the unconfined element is mostly composed of bioturbated very fine-grained sandstones and siltstones; this element is locally cut by a poorly channelized element (FC1), which becomes thicker laterally (out of view). D) Detailed view of the lowermost part of an unconfined heterolithic element (Arén sector, interval 3); this element is separated from the underlying overbank mudrocks by a slightly irregular 5th-order bounding surface (5); the basal strata of the unconfined element correspond to sandstones with high- to low-angle cross-bedding (Sp-Sl lithofacies) passing upward to very fine-grained sandstones to siltstones (Fl lithofacies). Due to their original content of organic remains, these sandstones show frequent irregular reduction spots (arrows).

ability to travel great distances over low slopes (Costa, 1984). Despite the low content of mud, some subaerial sediment gravity flows can move downslope as lobes (Mulder and Alexander, 2001), and they can exhibit concentrations of coarse clasts in their marginal parts when they accumulate as terminal lobes (Costa, 1984); the lenses and blankets of disorganized conglomerates described here might be comparable to such lobes. The limited occurrence of horizontally stratified conglomerates or sandstones on top of these massive bodies could be due to streamflow reworking (Nemec and Steel, 1984).

6.3. Fluvial non-channelized deposits

Fluvial non-channelized deposits are the dominant constituent component of the Upper Red Garumnian: they form around 85% of the measured stratigraphic sections. Based on their geometry and constituent lithofacies, two main architectural-element types have been distinguished: (i) unconfined heterolithic elements (FH) and (ii) mud-prone overbank elements (FM).

6.3.1. Unconfined heterolithic elements (FH)

6.3.1.1. Description. Unconfined heterolithic elements (FH) are a notable component of the studied Upper Red Garumnian deposits, forming ~24% of the measured sections and being identified in the four defined stratigraphic intervals. These elements are most commonly located directly adjacent to or overlying channelized or debris-flow bodies. Locally, tabular bodies with similar sedimentological features, but without any observed spatial relationship with coarser-grained deposits, are also seen. In downstream (SE to SSW) profiles, these elements present a tabular (Fig. 13A) to wedge-shaped morphology (Fig. 13B); despite the good continuity of the exposures, sections oriented parallel to depositional strike are not sufficiently continuous to enable assessment of the lateral extent of these bodies; however, considering the dimensions of the underlying coarse-grained bodies, the FH elements can probably attain apparent width values from 5 to 70 m. Their maximum thickness is from less than 1 m to 13.5 m, but is typically less than 6 m. Where FH elements overlie channelized bodies, their lower boundary can correspond to low-relief, accretionary 4th-order surfaces (Fig. 13A and C); instead, where located above overbank elements, this basal boundary is usually erosional and sharp, and can be ranked as a 5th-order surface (Fig. 13B and D). In their downstream terminations, these elements can pinch out within overbank elements (Fig. 13A).

The FH elements are mostly composed of well stratified (planar-horizontally stratified to ripple laminated) to massive (mainly bioturbated) interbeds of very fine-grained sandstones and siltstones (lithofacies Fl: 92.7%); thin (less than 0.5 m) interbeds of horizontal-bedded (Sh: 2.8%) and massive sandstones (Sm: 3.4%) are other significant components; cross-bedded sandstones were not recorded in the measured sections, but are observed locally (Fig. 13D). Local load structures are observed below such coarser-grained interbeds. The effects of bioturbation and pedogenesis are common features of these deposits. The bioturbation of beds is variable, ranging in form from discrete burrows to completely homogenized beds. Biogenic structures comprise mainly subvertical regular cylindrical burrows, although rare burrows that are meniscate, else that show midway enlargements, are observed in places. In highly bioturbated strata, horizontal burrows are also common. Common pedogenic features of these deposits, although usually restricted to red-coloured strata, are reduction spots and mottles, branched rhizohaloes, and leaf imprints (see below for additional details).

6.3.1.2. Interpretation. Considering their fine-grained size and the conspicuous occurrence of planar and ripple-lamination, the FH elements can be interpreted as the result of unconfined, decelerating, shallow-water flows in a low-relief and low-gradient alluvial-plain setting (Hubert and Hyde, 1982; Wells, 1983; Sadler and Kelly, 1993). Such overbank flows caused deposition of fine-grained bedload at the transition between lower and upper flow-regimes, along with suspended sediments (Hubert and Hyde, 1982; Stear, 1983; Parkash et al., 1983; Gulliford et al., 2014). In present-day dryland areas, the deposits of overland flows are associated with relatively high-frequency and low-magnitude flood events (Vyverberg, 2010). The preserved record of such overbank flooding events is mainly represented by wide, elongate, sheet-like bodies commonly referred to as splay deposits (Stear, 1983; McKie, 2011; Gulliford et al., 2014; Wilson et al., 2014). In modern dryland areas, similar unconfined deposits are located at the termini of rivers, where they form so-called terminal splays (Abdullatif, 1989; Fisher et al., 2008; Coronel et al., 2020; Li et al., 2020). The location of these deposits above the channelized elements suggest that this type of sedimentation became important once these channels were completely infilled (Schumm, 1961). In addition, their gradation to channelized deposits may indicate that the unconfined lobes were fed upstream by such channelized systems (McKie and Audretsch, 2005). Pervasive biogenic or pedogenic alteration is commonly observed in recent and ancient examples of similar deposits, and is associated with the time between flood events (Fisher et al., 2008; McKie, 2011; Burns et al., 2017). The observed vertical burrows may correspond to shelter traces, whereas horizontal burrows are typically associated with feeding processes (Hasiotis, 2002). The presence of rhizohaloes, slickensides and wedge-shaped peds suggests that, despite the dominant well-drained conditions, fluctuations in soil saturation took place. Where spatial relationships with presumed genetically related channel deposits cannot be observed, these deposits might correspond to the most distal parts of elements of this type.

6.3.2. Mud-prone overbank elements (FM)

6.3.2.1. Description. Mud-prone overbank elements (FM) are the most abundant deposits in the Upper Red Garumnian, constituting ca. 80% of the entire studied succession; they are ubiquitous in the four defined stratigraphic intervals. FM elements extend laterally over hundreds of metres, and in the measured sections can locally attain up to 70 m in thickness. Where located above FH elements, the lower contact can be gradational.

The lithofacies of mudstones and siltstones (Fsm) is by far the dominant component of FM elements attaining an abundance of 98.7%; other components are present with abundances lower than 1% and comprise thin to medium beds (<0.5 m) of very-fine grained sandstones to siltstones (Fl: 0.5%), massive to horizontally bedded sandstones (Sm: 0.2% and Sh: 0.1% respectively), and horizontally bedded conglomerates (Gh: 0.1%); pedogenic calcareous nodules (P lithofacies) occur locally in a similar low percentage (0.2%). The dominant fine-grained sediments show different degrees of pedogenic alteration, which produced palaeosols with a characteristic horizonation due to different intensities of redoximorphic features (mottling; Fig. 14a and B). Burrows and drab-haloed root traces are relatively common in these deposits. Gypsum (Fig. 14C) occurs mainly as irregular aggregates (<10 cm of major dimension) of anhedral crystals, or less commonly as laminar aggregates and veinlets that probably originated by reprecipitation. Although the occurrence of gypsum is usually observed at different locations and stratigraphic levels, locally, in the western part of the Esplugafreda section and in the upper part of interval 2, such accumulations attain a higher concentration (Fig. 4), which can even be observed in aerial orthophotographs. In the outcrops near Gurp, these gypsum accumulations are locally very abundant (Fig. 14C). Calcareous nodules (individually less than 2 cm) are present as accumulations in distinct horizons. A discrete carbonate layer is observed (Fig. 14D) that is less than 0.5 m thick; although discontinuous, it appears in segments with up to 100 m of lateral continuity; this layer is located in the middle part of interval 2 and is composed of massive to banded limestones, which locally show a nodular habit and lack macroscopic evidence of fossil content.

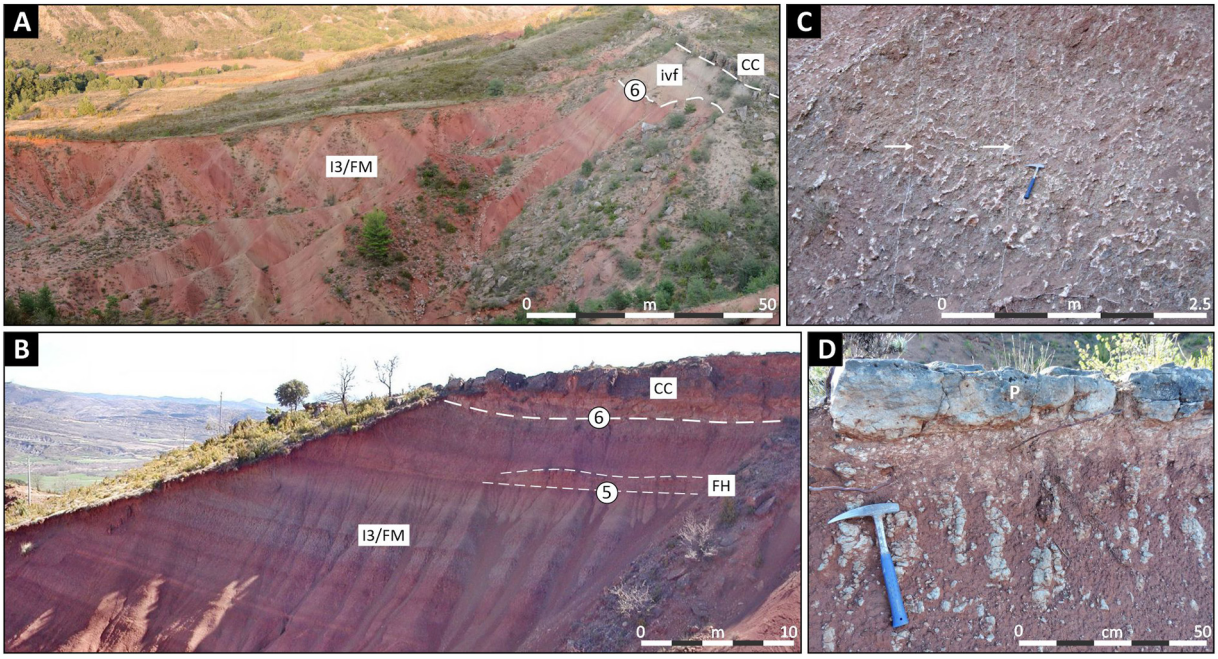

Fig. 14. Outcrop examples of overbank deposits. A) Oblique view of monotonous overbank deposits (I3/FM) constituting the uppermost part of the interval 3 in the Esplugafreda sector; the irregular contact with an incised valley fill (ivf) in the base of the interval 4 corresponds to a 6th-order bounding surface; the Claret Conglomerate overlies this valley fill. B) Oblique view of overbank deposits (I3/FM) from the uppermost part of the interval 3 in the Arén sector, overlain directly by the Claret Conglomerate (CC); the overbank deposits show a characteristic palaeosol horizonation; locally an unconfined heterolithic element (FH) is interposed within these overbank deposits; the base of this heterolithic element corresponds to a horizontal 5th-order bounding surface whilst its top is convex and gradational. C) Detail of overbank deposits (Gurp sector) rich in gypsum aggregates; the gypsum has been locally reprecipitated in planar veins (arrows). D) Detail view of overbank deposits (Esplugafreda sector, interval 2) with tabular palustrine carbonates (P lithofacies); below these carbonates, the overlying mudrocks (Fsm lithofacies) contain rhizoliths and carbonate nodules.

6.3.2.2. Interpretation. Based on their grain size and overall architecture, these deposits record suspension settling associated with overbank floods flowing over distal floodplain areas to develop mudflats (Parkash et al., 1983; Stear, 1983; Wells, 1983; Cowan, 1993; Coronel et al., 2020). The episodic, but apparently frequent flooding of such areas, which covered the major part of this fluvial system, lead to the accumulation of thick and wide mud-prone successions (Parkash et al., 1983; Stear, 1983; Ghosh and Sarkar, 2011). Possible periodic flooding may be responsible for the differential mottling and banded aspects of these deposits, in relation to seasonal differences in soil saturation (Kraus, 1992). Palaeosols in the studied sections have been classified as Vertisols, but Aridisols may also be present (Fjellbirkeland, 1990). The presence of rhizoliths in these deposits suggests the existence of some vegetation, a feature common of floodplains in dryland areas (Scott, 2006; Bridge and Demicco, 2008). Gypsum precipitates in this succession were previously associated with evaporation cycles and arid conditions (Fjellbirkeland, 1990); however, a pedogenic origin mediated by bacterial activity may be more likely in view of their concentration in root holes and along slickensides fractures. The formation of Bk horizons enriched in pedogenic carbonate nodules may reflect carbonate precipitation in a floodplain setting experiencing a negative water balance and a gap in sedimentation, whereas the carbonate bed of interval 2 may represent carbonate precipitation in a palustrine setting subject to negligible input of clastic sediment (cf. Alonso-Zarza and Wright, 2010; Arostegi et al., 2011).

7. Discussion

The Upper Red Garumnian succession in the study area comprises mostly non-channelized fluvial elements resulting from sedimentation via unconfined mud-laden flows, principally in overbank settings neighbouring fluvial channels and represented by widespread mudflats. Based on the proportion of these deposits in the measured vertical sections, and the available chronostratigraphic framework, these alluvial mudflats were the dominant landscape in the late Paleocene in the eastern part of the Tremp-Graus basin. The channelized elements are variably distributed depending on their stratigraphic position: they tend to be broadly scattered in intervals 1 and 2, formed during a stage of tectonic quiescence; by contrast, they tend to be dominantly clustered, in some cases within palaeovalleys, in interval 3 and in the lowermost part of interval 4, as a result of changes in streambed graded profile related to reactivated uplift (Fernández et al., 2012) and eustatic changes (valley fills of Pujalte et al., 2014; cf. Colombera et al., 2017; Fig. 4). Following the onset of the PETM, with a temporal lag in the order of 4000 years (Pujalte et al., 2022) to 10^5 years (Duller et al., 2019), the fluvial style in this part of the basin changed drastically: during the earliest Eocene, channel belts migrated rapidly across the alluvial plain causing the cannibalization of floodplain areas, as well as the erosional planation of palaeotopographic highs (Colombera et al., 2017); after the PETM recovery, these alluvial environments reverted to their mud-prone character, under conditions of increased proximity to the coast, which heralded the establishment of marine conditions recorded by the early Eocene Alveolina Limestone and equivalent facies.

The documented changes in the stratigraphic architecture of the Upper Red Garumnian reflect the variable role of allogenic drivers, specifically tectonics and climate, which resulted from global scale processes (PETM) to more basin-wide controls (multistage uplift of the Pyrenees). Meanwhile, at a smaller scale, sedimentological observations from channelized elements reveal the influence of discharge variability as a control on facies architectures.

In most channelized elements, there is evidence of deposition by streams with significant water-discharge variability; locally, evidence of physical and biogenic processes of sediment alteration (burrowing, desiccation and root growth; Fig. 15) indicate ephemeral or intermittent discharge. The predominance of high-stage and upper-flow regime bedforms, mostly horizontally bedded sandstones and conglomerates,

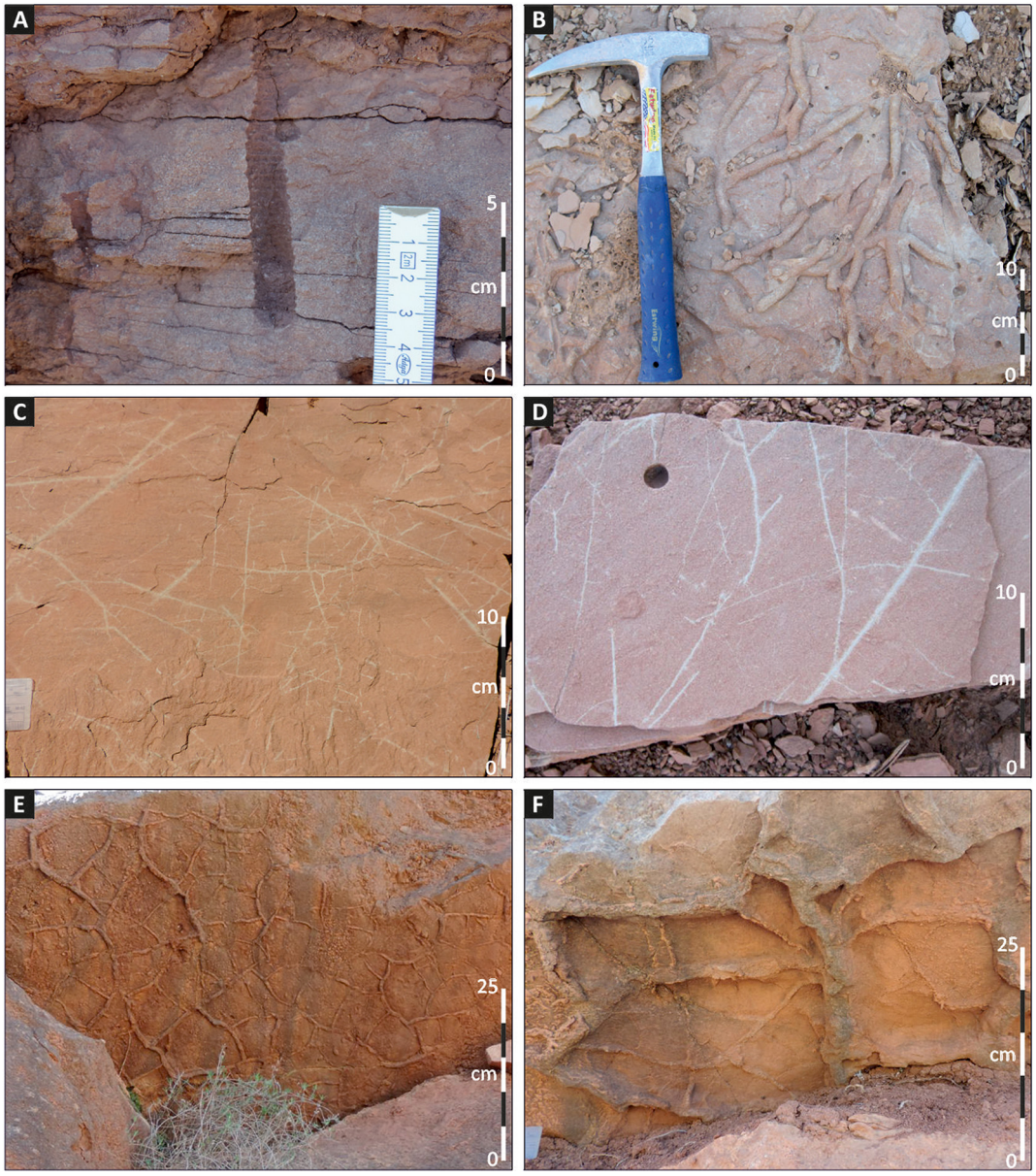

Fig. 15. In-channel sedimentary features diagnostic of streamflow interruption in deposits of fluvial channels subject to high variability in discharge. Most of these features are associated with horizontally laminated sandstones. A) Meniscate vertical burrow. B) Branched horizontal burrows. C–D) Horizontal rhizohaloes. E–F) Casts of desiccation cracks, located at the base of sandstone bodies, and above thin interbeds of muddy lithofacies.

reflects the prevalence of shallow rapid flows. The intermittent nature of water discharge is additionally testified by the limited reworking of rapidly aggraded channel deposits. Certain diagnostic characteristics of rivers with highly variable discharge, such as partially buried stumps and trees (Fielding et al., 2018), are lacking; nonetheless, possible evidence of sparse vegetation colonizing the channel beds during low flow stages or droughts may be recorded by the preservation of extensive networks of sub-horizontal rhizohaloes (Fig. 15C and D).

The simple single-storey elements (FC1), which are frequently dominated by a single lithofacies and tend to lack reactivation surfaces or mud drapes, are interpreted as the product of channel inception and infill by a single flood. Elements of this type are thought to represent the infill of fluvial channels located in overbank-dominated alluvial-plain areas, either as isolated channels incising overbank deposits (FM), or as flow conduits that developed in the late stages of accumulation of genetically related unconfined heterolithic elements (FH). For compound single-storey elements (FC2), a detailed characterization of their internal architecture is hampered by the fact that most exposures have limited three-dimensional control; most outcropping sections are oriented approximately perpendicular to the average palaeoflow direction. Nonetheless, a record of multiple flood events affecting the same channel forms is identified in the vertical stacking of m-scale deposits of individual floods, dominated by sandy to gravelly bedforms and sand sheets deposited during high flow stages and overlain by cm- to dm-scale drapes of fine-grained sandstones and siltstones deposited by suspension settling during waning stages. Bioturbation affects the fining-upward and sandstone packages of these elements, which is especially significant in view of their inherently high water-holding capacity. Multi-storey and multilateral elements (FC3) represent the deposits of channel belts with a more complex morphodynamic evolution, encompassing the dissection and reworking of previous coarse-grained deposits and occasional channel widening; these FC3 elements tend to form the basal portion of major fining-upward successions. The channel belts that formed these bodies comprised of bedforms and

elements of different types and scales, such as unit bars, gravelly and sandy bedforms, plane beds, as well as channel fills; individual storeys can be separated by scour surfaces with metric relief. Macroform-accretion geometries are particularly evident in FC2 and FC3 elements from the lower part of interval 4, including and up to the Claret Conglomerate, in conjunction with a larger fraction of facies relating to mesoform-scale bedforms. This architectural change may indicate a transition to more perennial conditions (Colombera et al., 2017; cf. Plink-Björklund, 2015; Fielding et al., 2018). A substantial change in the type of lithofacies forming the Claret Conglomerate, relative to the underlying deposits of interval 4, is not seen. Yet, the Claret Conglomerate, which is a particular type of FC3 element, marks a sudden increase in the apparent width of the channelized elements (cf. Dreyer, 1993; Schmitz and Pujalte, 2007; Colombera et al., 2017). The local occurrence of fine-grained elements of limited lateral extension suggests that the change in architecture (size and stacking pattern of channel bodies) may reflect increased channel mobility and avulsion frequency.

A limited proportion of the Upper Red Garumnian in the study area is made of deposits of sediment gravity-flows, represented by clast-supported disorganized bodies, which are mostly stratigraphically limited to the basal part of the stratigraphic interval 2. The interfingering of debris-flow deposits with fine-grained fluvial deposits has been locally reported in the Munster Basin of southern Ireland (Graham, 1983), which has been referred to as an example of an alluvial basin where debris-flow processes coexisted with braided-river deposition (Stanistreet and McCarthy, 1993). Additionally, the significant occurrence of conglomeratic deposits in relatively distal parts of this alluvial system can be related to an intrinsic factor of this sedimentary basin, namely the dominance of carbonates in the source area (Fjellbirkeland, 1990). Similar conditions are seen in modern alluvial systems developed under arid and semiarid climatic conditions in central Texas, where streams associated with limestone terrains are associated with coarse gravel and boulders that are mobilized during major floods (Baker, 1977).

The overbank deposits, which constitute the 85% of the succession in the study area, were formed by overbank flows during major seasonal floods or by low-energy but high-frequency mud-laden flows. Unconfined flows are dominated by very fine-grained sandstone and coarse-grained siltstone deposits, which usually show evidence of pedogenesis, including the common occurrence of burrows and rhizoliths. These characteristics might be related to transient water saturation of the soil, and to the development of riparian ecosystems. In overbank deposits, the pedogenesis is more strongly controlled by cycles of drying and wetting, and includes the development of mottled patterns and the precipitation of calcareous nodules and gypsum aggregates. Analysis of palaeosol characteristics indicates the predominance of a dry climate, important seasonal variations in moisture, as well as a progressive increase in precipitation through the time of interval 3. The red-coloured nature of the overbank deposits of intervals 1 to 3 suggests prevailing well-drained conditions during the deposition of most of the Upper Red Garumnian. Nonetheless, in the lower part of interval 4, (members 1 to 2 of the Claret Formation of Baceta et al., 2011), the occurrence of grey-coloured fine-grained deposits with coaly fragments testifies to the existence of waterlogged areas that enabled organic matter preservation in relation to reducing conditions. In addition, the conglomeratic deposits forming the amalgamated complexes of the Claret Conglomerate of Baceta et al. (2011) contain oncolites (Fig. 16), which may be associated with shallow ponded areas neighbouring or within the channel belts that produced the coarse-grained bodies. These features indicate that the lower interval 4 recorded a change to poorly drained conditions, which could also be responsible for the apparently higher degree of cementation observed in the conglomeratic deposits of this interval, due to a shallower phreatic zone. A water-table rise would have occurred as part of a long-term trend of palaeohydrological change that predated the onset of the PETM, and which is expressed in interval 3 in palaeosol characteristics that indicate a seasonal increase in precipitation. Overall, this may reflect some progressive intensification of the hydrologic cycle in the study area during the late Paleocene warming trend (cf. Bice and Marotzke, 2002; Kender et al., 2012).

To summarize our sedimentological characterization of the succession, a sedimentological model is proposed for the Upper Red Garumnian (Fig. 17) that depicts schematically the distribution of the architectural elements across the four described intervals. Compound single-storey (FC2) and amalgamated complexes (FC3) are associated with wide areas of unconfined heterolithic deposits. Debris-flow elements (DF) are only found in the interval 2, and specifically at its base. Palaeosol horizons with calcareous nodules are common in mud-prone overbank deposits, particularly those of the interval 2. The base of the interval 3 is marked by local amalgamated complexes, but in overlying strata the channelized bodies tend to be clustered (Figs. 3, 4), suggesting the influence of topographic (e.g., valley confinement) or autogenic (e.g., presence of avulsion nodes) controls on their distribution (cf. Hajek et al., 2010). The Claret Conglomerate records channel-belt amalgamation by lateral migration of individual channels. Poorly drained conditions are locally interpreted for the Claret Conglomerate and the underlying lower interval 4 deposits in the Esplugafreda area, where ponded areas within channel belts and water-logged zones in overbank areas existed.

In summary, variations in water discharge are recognized to have occurred over a range of timescales (from that of flood events to that of the late Paleocene warming trend): these left distinctive sedimentary records at corresponding spatial scales (from that of the lithofacies to

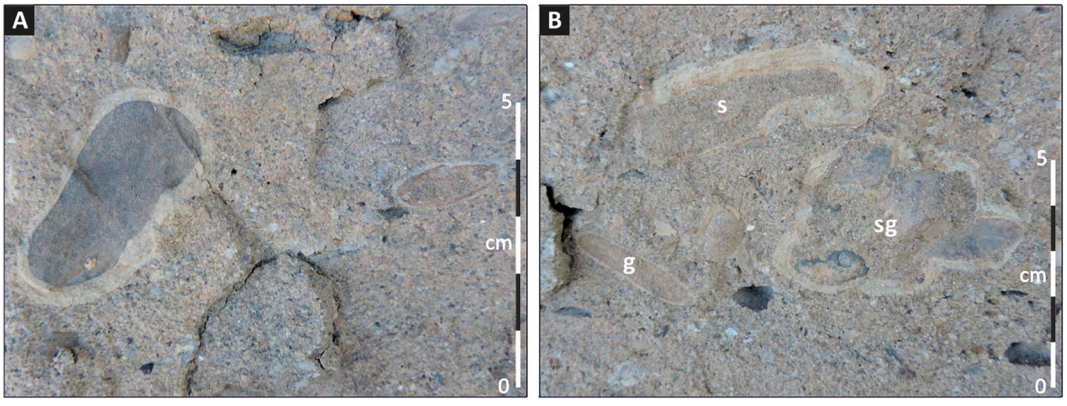

Fig. 16. Oncolites from the Claret Conglomerate related to the development of ponded areas within channel belts. A) Oncolites formed around individual nuclei of gravel-sized fragments. B) Besides of being formed around individual gravel-size clasts (g), oncolites are also formed around lumps of sand (s) or sandy gravel (sg).

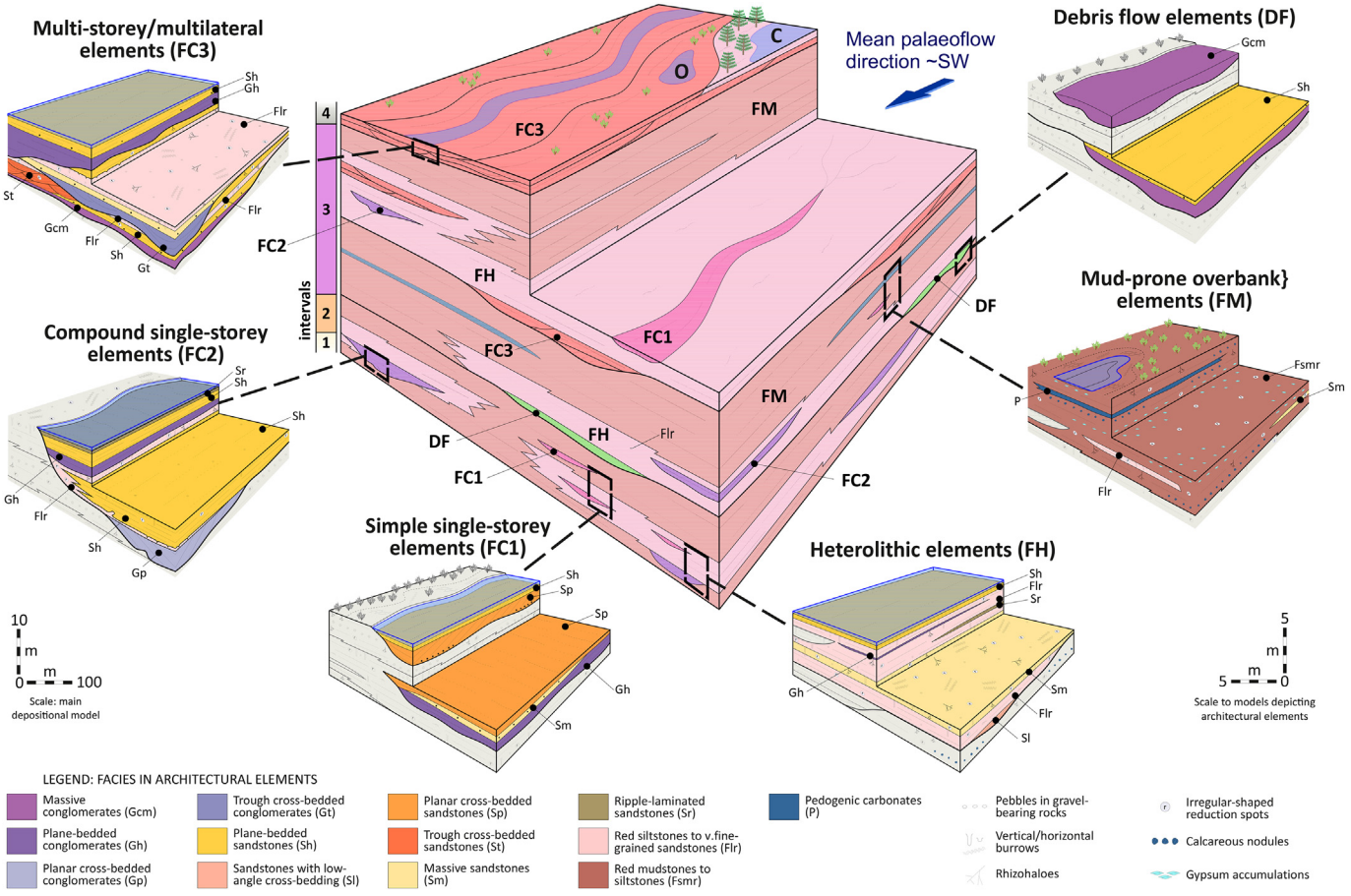

Fig. 17. Schematic sedimentological model for the Upper Red Garumnian in the Arén and Esplugafreda sector. To enable depiction of representative features of all stratigraphic intervals, the thickness of the intervals (I1 to I4) is not to scale; the top of the block is representative of the lower to mid part of interval 4. The parent block represents the distribution of architectural elements through the stratigraphy, whereas the smaller inset blocks display the distribution of lithofacies within architectural elements. Deposits belonging to elements of a different type are greyed-out in the detailed inset blocks. O: Ponded areas within channel belts of the lower interval 4 (Claret Conglomerate) where oncolites were formed; C: Water-logged areas in overbank area where accumulation of grey mudrocks with coaly fragments took place.

that of the entire Upper Red Garumnian), which indicate that climate was a prime control on the flow characteristics, depositional processes, channel morphodynamics, palaeosol development and topographic evolution of the studied alluvial system. To elucidate the significance and magnitude of the inferred environmental change, however, it is recommended that quantitative palaeohydraulic and palaeohydrological reconstructions (cf. Paredes et al., 2018; Long, 2021; Barefoot et al., 2022), ideally supported by geochemical analyses (cf. Sheldon et al., 2002), are undertaken.

8. Conclusions

Based on the analysis of its architecture and lithofacies characteristics, the late Paleocene to earliest Eocene fluvial succession exposed in the Arén-Esplugafreda sector – the Upper Red Garumnian– is shown to have characteristics comparable to those of the distal parts of other ancient and modern fluvial systems developed in dryland environments. Based on field mapping and the measurement of stratigraphic sections, four stratigraphic intervals (1 to 4 from base to top) have been defined in this succession. Channelized architectural elements comprise coarse-grained bodies produced by both streamflow and sediment gravity-flow processes; they account for ca. 15% of the cumulative measured stratigraphy, and exhibit significant variability in external geometries and styles of internal architecture. The Upper Red Garumnian is, however, dominated by fine-grained non-channelized strata that formed over wide areas of the original alluvial plain.

A detailed analysis of the stratigraphic architecture and facies organization of these deposits has revealed how water-discharge variations at different temporal scales acted as a fundamental control on the characteristics and evolution of this alluvial system. Facies arrangements and evidence of streambed drying are documented: these record the effects of highly variable discharge in ephemeral or intermittent channels, over timescales ranging from that of flood events to that of channel-form lifespans. Variations in facies assemblages, stratigraphic architecture and palaeosol characteristics through the stratigraphy testify to longer-term variations in channel morphodynamics, discharge regime, floodplain processes and pedogenesis; since these may reflect major hydrological changes in the late Paleocene and earliest Eocene, the findings of this work help improve our understanding of environmental change leading to, and including, the PETM.

Declaration of competing interest

The authors declare that they have no known competing financial interests or personal relationships that could have appeared to influence the work reported in this paper.

Acknowledgements

We thank the sponsors and partners of the Fluvial, Eolian & Shallow-Marine Research Group (AkerBP, Anadarko, Areva [now Orano], BHPBilliton, Cairn India [Vedanta], Chevron, ConocoPhillips, Equinor,

Murphy Oil, Nexen-CNOOC, Occidental, Petrotechnical Data Systems [PDS], Saudi Aramco, Shell, Tullow Oil, Woodside and YPF) for financial support to this research. We thank José Matildo Paredes, an anonymous reviewer, and Editor Catherine Chagué for their useful comments, which have improved this paper.

References

Abdullatif, O.M., 1989. Channel-fill and sheet-flood facies sequences in the ephemeral terminal River Gash, Kassala, Sudan. Sedimentary Geology 63, 171–184.

Adatte, T., Khozyem, H., Spangenberg, J.E., Samant, B., Keller, G., 2014. Response of terrestrial environment to the Paleocene-Eocene Thermal Maximum (PETM), new insights from India and NE Spain. Rendiconti Online della Società Geologica Italiana 31, 5–6.

Allen, J.P., Fielding, C.R., Gibling, M.R., Rygel, M.C., 2014. Recognizing products of palaeoclimate fluctuation in the fluvial stratigraphic record: an example from the Pennsylvanian to Lower Permian of Cape Breton Island, Nova Scotia. Sedimentology 61, 1332–1381.

Alonso-Zarza, A.M., Wright, V.P., 2010. Palustrine carbonates. In: Alonso-Zarza, A.M., Tanner, L.H. (Eds.), Developments in Sedimentology 61. Elsevier, Amsterdam, pp. 103–131.

Ardèvol, L., Klimowitz, J., Malagón, J., Nagtegaal, P.J., 2000. Depositional sequence response to foreland deformation in the Upper Cretaceous of the Southern Pyrenees, Spain. AAPG Bulletin 84, 566–587.

Arenas-Abad, C., Vázquez-Urbez, M., Pardo-Tirapu, G., Sancho-Marcén, C., 2010. Fluvial and associated carbonate deposits. In: Alonso-Zarza, A.M., Tanner, L.H. (Eds.), Developments in Sedimentology 61. Elsevier, Amsterdam, pp. 133–175.

Arostegi, J., Baceta, J.I., Pujalte, V., Carracedo, M., 2011. Late Cretaceous—Palaeocene mid-latitude climates: inferences from clay mineralogy of continental-coastal sequences (Tremp-Graus area, southern Pyrenees, N Spain). Clay Minerals 46, 105–126.

Baceta, J.I., Pujalte, V., Wright, V.P., Schmitz, B., 2011. Carbonate platform models, sea-level changes and extreme climatic events during the Paleocene/early Eocene greenhouse interval. In: Arenas, C., Pomar, L., Colombo, F. (Eds.), Pre-Meeting Field trips Guidebook, 28th IAS Meeting. Sociedad Geológica de España. Geo-Guías, Zaragoza, pp. 101–150.

Baker, V.R., 1977. Stream-channel response to floods, with examples from central Texas. Geological Society of America Bulletin 88, 1057–1071.

Barefoot, E.A., Nittrouer, J.A., Foreman, B.Z., Hajek, E.A., Dickens, G.R., Baisden, T., Toms, L., 2022. Evidence for enhanced fluvial channel mobility and fine sediment export due to precipitation seasonality during the Paleocene-Eocene thermal maximum. Geology 50, 116–120.

Bice, K.L., Marotzke, J., 2002. Could changing ocean circulation have destabilized methane hydrate at the Paleocene/Eocene boundary? Paleoceanography 17, 8 1.

Blair, T.C., McPherson, J.G., 1994. Alluvial fans and their natural distinction from rivers based on morphology, hydraulic processes, sedimentary processes, and facies assemblages. Journal of Sedimentary Research 64, 450–489.

Blair, T.C., McPherson, J.G., 1999. Grain-size and textural classification of coarse sedimentary particles. Journal of Sedimentary Research 69, 6–19.

Blair, T.C., McPherson, J.G., 2009. Processes and forms of alluvial fans. Geomorphology of Desert Environments. Springer, pp. 413–467.

Bond, R., McClay, K., 1995. Inversion of a Lower Cretaceous extensional basin, south central Pyrenees, Spain. Geological Society, London, Special Publications 88, 415–431.

Braunstein, J., 1961. Calciclastic and siliciclastic. AAPG Bulletin 45, 2017.

Bridge, J., Demicco, R., 2008. Earth Surface Processes, Landforms and Sediment Deposits. Cambridge University Press, New York (830 pp.).

Bromley, M.H., 1991. Variations in fluvial style as revealed by architectural elements, Kayenta Formation, Mesa Creek, Colorado, USA: Evidence for both ephemeral and perennial fluvial processes. In: Miall, A.D., Tyler, N. (Eds.), The Three-Dimensional Facies Architecture of Terrigenous Clastic Sediments and Its Implications for Hydrocarbon Discovery and Recovery. SEPM, pp. 94–102.

Burns, C.E., Mountney, N.P., Hodgson, D.M., Colombera, L., 2017. Anatomy and dimensions of fluvial crevasse-splay deposits: examples from the Cretaceous Castlegate Sandstone and Neslen Formation, Utah, USA. Sedimentary Geology 351, 21–35.

Butler, R.W., 1982. The terminology of structures in thrust belts. Journal of Structural Geology 4, 239–245.

Cain, S.A., Mountney, N.P., 2009. Spatial and temporal evolution of a terminal fluvial fan system: the Permian Organ Rock Formation, South-east Utah, USA. Sedimentology 56, 1774–1800.

Cámara, P., Klimowitz, J., 1985. Interpretación geodinámica de la vertiente centro-occidental surpirenaica (cuencas de Jaca-Tremp). Estudios Geológicos 41, 391–404.

Capote, R., Muñoz, J., Simón, J., Liesa, C., Arlegui, L., 2002. Alpine tectonics I: the Alpine system north of the Betic Cordillera. In: Gibbons, W.M., M. T. (Eds.), The Geology of Spain. Geological Society, London, pp. 367–400.

Chen, C., Guerit, L., Foreman, B.Z., Hassenruck-Gudipati, H.J., Adatte, T., Honegger, L., Perret, M., Sluijs, A., Castelltort, S., 2018. Estimating regional flood discharge during Palaeocene-Eocene global warming. Scientific Reports 8, 1–8.

Choukroune, P., 1992. Tectonic evolution of the Pyrenees. Annual Review of Earth and Planetary Sciences 20, 143–158.

Cojan, I., 1993. Alternating fluvial and lacustrine sedimentation: tectonic and climatic controls (Provence Basin, S. France, Upper Cretaceous/Palaeocene). In: Marzo, M., Puidefabregas, C. (Eds.), Alluvial Sedimentation. IAS Special Publicationvol. 17, pp. 425–438.

Colombera, L., Mountney, N.P., 2019. The lithofacies organization of fluvial channel deposits: a meta-analysis of modern rivers. Sedimentary Geology 383, 16–40.

Colombera, L., Mountney, N.P., McCaffrey, W.D., 2013. A quantitative approach to fluvial facies models: methods and example results. Sedimentology 60, 1526–1558.

Colombera, L., Arévalo, O.J., Mountney, N.P., 2017. Fluvial-system response to climate change: the Paleocene-Eocene Tremp group, Pyrenees, Spain. Global and Planetary Change 157, 1–17.

Coronel, M.D., Isla, M.F., Veiga, G.D., Mountney, N.P., Colombera, L., 2020. Anatomy and facies distribution of terminal lobes in ephemeral fluvial successions: Jurassic Tordillo Formation, Neuquén Basin, Argentina. Sedimentology 67, 2596–2624.

Costa, J.E., 1984. Physical geomorphology of debris flows. In: Costa, J.E., Fleisher, P.J. (Eds.), Developments and Applications of Geomorphology. Springer, pp. 268–317.

Costa, J.M., Maestro-Maideu, E., Betzler, C.H., 1996. The Paleogene basin of the Eastern Pyrenees. In: Friend, P.F., Dabrio, C.J. (Eds.), Tertiary Basins of Spain: The Stratigraphic Record of Crustal Kinematics. Cambridge University Press, Cambridge, pp. 106–113.

Cowan, G., 1993. Identification and significance of aeolian deposits within the dominantly fluvial Sherwood Sandstone Group of the East Irish Sea Basin UK. In: North, C.P., Prosser, D.J. (Eds.) Characterization of Fluvial and Aeolian Reservoirs. Geological Society, London, Special Publications 73, 231–245.

Cuevas, J.L., 1992. Estratigrafía del "Garumniense" de la Conca de Tremp. Prepirineo de Lérida. Acta Geologica Hispánica 27, 95–108.

Dawson, A., Grimes, S., Ellis, M., Duller, R., Watkinson, M., Stokes, M., Leng, M.J., 2014. Initial paleohydrological observations from the Paleocene-Eocene boundary at Esplugafreda and Berganuy in northern Spain. Rendiconti Online della Società Geologica Italiana 31, 54–55.

Domingo, L., López-Martínez, N., Leng, M.J., Grimes, S.T., 2009. The Paleocene–Eocene Thermal Maximum record in the organic matter of the Claret and Tendruy continental sections (South-central Pyrenees, Lleida, Spain). Earth and Planetary Science Letters 281, 226–237.

Donaire, M., López-Martínez, N., 2009. Porosity of late paleocene ornitholithus eggshells (Tremp Fm, south-Central Pyrenees, Spain): palaeoclimatic implications. Palaeogeography, Palaeoclimatology, Palaeoecology 279, 147–159.

Dreyer, T., 1993. Quantified fluvial architecture in ephemeral stream deposits of the Esplugafreda Formation (Palaeocene), Tremp-Graus Basin, northern Spain. In: Marzo, M., Puidefabregas, C. (Eds.), Alluvial Sedimentation. IAS Special Publicationvol. 17, pp. 337–362.

Duller, R.A., Armitage, J.J., Manners, H.R., Grimes, S., Jones, T.D., 2019. Delayed sedimentary response to abrupt climate change at the Paleocene-Eocene boundary, northern Spain. Geology 47, 159–162.

Feist, M., Colombo, F., 1983. La limite Crétacé-Tertiaire dans le nord-est de l'Espagne, du point de vue des charophytes. Géologie Méditerranéenne 10, 303–326.

Fernández, O., Muñoz, J.A., Arbués, P., Falivene, O., 2012. 3D structure and evolution of an oblique system of relaying folds: the Ainsa basin (Spanish Pyrenees). Journal of the Geological Society 169, 545–559.

Fielding, C.R., 2006. Upper flow regime sheets, lenses and scour fills: extending the range of architectural elements for fluvial sediment bodies. Sedimentary Geology 190, 227–240.

Fielding, C.R., Allen, J.P., Alexander, J., Gibling, M.R., 2009. Facies model for fluvial systems in the seasonal tropics and subtropics. Geology 37, 623–626.

Fielding, C.R., Alexander, J., Allen, J.P., 2018. The role of discharge variability in the formation and preservation of alluvial sediment bodies. Sedimentary Geology 365, 1–20.

Fisher, J.A., Krapf, C.B., Lang, S.C., Nichols, G.J., Payenberg, T.H., 2008. Sedimentology and architecture of the Douglas Creek terminal splay, Lake Eyre, central Australia. Sedimentology 55, 1915–1930.

Fjellbirkeland, H., 1990. Tidlig diagenese og pedogenese under semi-aride forhold: Esplugafredaformasjonen og Claretformasjonen (paleocen) i Trempbassenget, Spanske Pyreneene. (MSc Thesis)University of Bergen.

Frostick, L.E., Reid, I., 1977. The origin of horizontal laminae in ephemeral stream channel-fill. Sedimentology 24, 1–9.

Ghosh, P., Sarkar, S., 2011. Pedogenic and sedimentologic criteria for recognition of overbank sub-environments in a Triassic anabranching-river deposit. In: Davidson, S.K., Leleu, S., North, C.P. (Eds.), From River to Rock Record: The Preservation of Fluvial Sediments and their Subsequent Interpretation. SEPM Special Publicationvol. 97, pp. 125–142.

Gibling, M.R., 2006. Width and thickness of fluvial channel bodies and valley fills in the geological record: a literature compilation and classification. Journal of Sedimentary Research 76, 731–770.

Gradstein, F.M., Ogg, J.G., Van Kranendonk, M., 2008. On the geologic time scale 2008. Newsletters on Stratigraphy 43, 5–13.

Graham, J.R., 1983. Analysis of the Upper Devonian Munster Basin, an example of a fluvial distributary system. In: Collinson, J.D., Lewin, J. (Eds.), Modern and Ancient Fluvial Systems. IAS Special Publicationvol. 6, pp. 473–483.

Gulliford, A.R., Flint, S.S., Hodgson, D.M., 2014. Testing applicability of models of distributive fluvial systems or trunk rivers in ephemeral systems: reconstructing 3-D fluvial architecture in the Beaufort Group, South Africa. Journal of Sedimentary Research 84, 1147–1169.

Hajek, E.A., Heller, P.L., Sheets, B.A., 2010. Significance of channel-belt clustering in alluvial basins. Geology 38, 535–538.

Hampton, B.A., Horton, B.K., 2007. Sheetflow fluvial processes in a rapidly subsiding basin, Altiplano plateau, Bolivia. Sedimentology 54, 1121–1148.

Hasiotis, S.T., 2002. Continental ichnology: using terrestrial and freshwater trace fossils for environmental and climatic interpretations. SEPM Short Course51.

Hassan, M.A., 2005. Characteristics of gravel bars in ephemeral streams. Journal of Sedimentary Research 75, 29–42.

Hassan, M.A., Marren, P.M., Schwartz, U., 2009. Bar structure in an arid ephemeral stream. Sedimentary Geology 221, 57–70.

Hirst, J., 1991. Variations in alluvial architecture across the Oligo-Miocene Huesca fluvial system, Ebro Basin, Spain. In: Miall, A.D., Tyler, N. (Eds.), The Three-Dimensional

Facies Architecture of Terrigenous Clastic Sediments and Its Implications for Hydrocarbon Discovery and Recovery. SEPM, pp. 111–121.
Horiuchi, Y., Hisada, K.I., Lee, Y.I., 2009. Paleosol profiles in the Shiohama Formation of the lower cretaceous Kanmon Group, Southwest Japan and implications for sediment supply frequency. Cretaceous Research 30, 1313–1324.
Hubert, J., Hyde, M., 1982. Sheet-flow deposits of graded beds and mudstones on an alluvial sandflat-playa system: Upper Triassic Blomidon redbeds, St Mary's Bay, Nova Scotia. Sedimentology 29, 457–474.
Jain, M., Tandon, S.K., Singhvi, A.K., Mishra, S., Bhatt, S.C., 2005. Quaternary alluvial stratigraphical development in a desert setting: a case study from the Luni River basin, Thar Desert of western India. In: Blum, M., Marriott, S., Leclair, S. (Eds.), Fluvial Sedimentology VII. IAS Special Publication35, pp. 349–371.
Karcz, I., 1972. Sedimentary structures formed by flash floods in southern Israel. Sedimentary Geology 7, 161–182.
Kender, S., Stephenson, M.H., Riding, J.B., Leng, M.J., Knox, R.W.B., Peck, V.L., Kendrick, C.P., Ellis, M.A., Vane, C.H., Jamieson, R., 2012. Marine and terrestrial environmental changes in NW Europe preceding carbon release at the Paleocene–Eocene transition. Earth and Planetary Science Letters 353, 108–120.
Kjemperud, A.V., Schomacker, E.R., Cross, T.A., 2008. Architecture and stratigraphy of alluvial deposits, Morrison formation (Upper Jurassic), Utah. AAPG Bulletin 92, 1055–1076.
Kraus, M.J., 1992. Alluvial response to differential subsidence: sedimentological analysis aided by remote sensing, Willwood Formation (Eocene), Bighorn Basin, Wyoming, USA. Sedimentology 39, 455–470.
Leary, K.C., Ganti, V., 2020. Preserved fluvial cross strata record bedform disequilibrium dynamics. Geophysical Research Letters 47 (2), e2019GL085910. https://doi.org/10.1029/2019GL085910.
Leymerie, A., 1868. Présence de garumnien en Espagne. Bulletin de la Société Géologique de France2 pp. 906–911.
Li, J., Vandenberghe, J., Mountney, N.P., Luthi, S.M., 2020. Grain-size variability of point-bar deposits from a fine-grained dryland river terminus, Southern Altiplano, Bolivia. Sedimentary Geology, 105663 https://doi.org/10.1016/j.sedgeo.2020.105663.
Lindholm, R., 1987. A Practical Approach to Sedimentology. Allen and Unwin, London.
Long, D.G., 2021. Trickling down the paleoslope: an empirical approach to paleohydrology. Earth-Science Reviews 220, 103740. https://doi.org/10.1016/j.earscirev.2021.103740.
López-Martínez, N., Peláez-Campomanes, P., 1999. New mammals from south-Central Pyrenees (Tremp Formation, Spain) and their bearing on late Paleocene marine-continental correlations. Bulletin de la Société Géologique de France 170, 681–696.
López-Martínez, N., Arribas Mocoroa, M.E., Robador, A., Vicens, E., Ardèvol, L., 2006a. Los carbonatos danienses (Unidad 3) de la FM Tremp (Pirineos Sur-Centrales) : paleogeografía y relación con el límite Cretácico-Terciario. Revista de la Sociedad Geológica de España 19, 233–255.
López-Martínez, N., Dinarés-Turell, J., Elez, J., 2006b. Chronostratigraphy of the continental Paleocene series from the South Central Pyrenees (Spain): new magnetostratigraphic constraints. Climate and Biota of the early Paleogene83. University of the Basque Country, Bilbao (volume of Abstracts).
Luterbacher, H., Eichenseer, H., Betzler, C., Van Den Hurk, A., 1991. Carbonate siliciclastic depositional systems in the Paleogene of the south Pyrenean foreland basin: a sequence stratigraphic approach. In: MacDonald, D.I.M. (Ed.), Sedimentation, Tectonics and Eustasy; Sea Level Changes at Active Margins. IAS Special Publicationvol. 12, pp. 391–407.
Manners, H.R., Grimes, S.T., Sutton, P.A., Domingo, L., Leng, M.J., Twitchett, R.J., Hart, M.B., Jones, T.D., Pancost, R.D., Duller, R., Lopez-Martinez, N., 2013. Magnitude and profile of organic carbon isotope records from the Paleocene–Eocene Thermal Maximum: evidence from northern Spain. Earth and Planetary Science Letters 376, 220–230.
McKee, E., Crosby, E., Berryhill Jr., H., 1967. Flood deposits, Bijou Creek, Colorado, June 1965. Journal of Sedimentary Petrology 37, 829–851.
McKie, T., 2011. Architecture and Behavior of Dryland Fluvial Reservoirs, Triassic Skagerrak Formation, Central North Sea. From River to Rock Record: The Preservation of Fluvial Sediments and their Subsequent Interpretation97 pp. 189–214.
McKie, T., Audretsch, P., 2005. Depositional and structural controls on Triassic reservoir performance in the Heron Cluster, ETAP, Central North Sea, Geological Society, London, Petroleum Geology Conference series. Geological Society of London, pp. 285–297.
Médus, J., 1977. Palynostratigraphie des zones à Alveolina primaeva A. levis et A. cucumiformis dans les Pyrénées. Géobios 10, 625–639.
Médus, J., Colombo, F., 1991. Succesion climatique et limite stratigraphique Crétacé-Tertiaire dans le NE de l'Espagne. Acta Geologica Hispánica 26, 173–179.
Mey, P., Nagtegaal, P., Roberti, K., Hartevelt, J., 1968. Lithostratigraphic subdivision of post-Hercynian deposits in the south-central Pyrenees, Spain. Leidse Geologische Mededelingen 41, 221–228.
Miall, A.D., 1978. Lithofacies types and vertical profile models in braided river deposits: a summary. In: Miall, A.D. (Ed.), Fluvial Sedimentology. Canadian Society of Petroleum Geology, Memoirvol. 5, pp. 597–604.
Miall, A.D., 1985. Architectural-element analysis: a new method of facies analysis applied to fluvial deposits. Earth-Science Reviews 22, 261–308.
Miall, A.D., 1996. The Geology of Fluvial Deposits: Sedimentary Facies, Basin Analysis, and Petroleum Geology. Springer, Berlin (582 pp.).
Mulder, T., Alexander, J., 2001. The physical character of subaqueous sedimentary density flows and their deposits. Sedimentology 48, 269–299.
Naylor, M., Sinclair, H., 2008. Pro-vs. retro-foreland basins. Basin Research 20, 285–303.
Nemec, W., Steel, R.J., 1984. Alluvial and coastal conglomerates: their significant features and some comments on gravelly mass-flow deposits. In: Koster, E.H., Steel, R.J. (Eds.), Sedimentology of Gravels and Conglomerates. Canadian Society of Petroleum Geologists, Memoirvol. 10, pp. 1–31.
Nijman, W., 1998. Cyclicity and basin axis shift in a piggyback basin: towards modelling of the Eocene Tremp-Ager Basin, South Pyrenees, Spain. In: Mascle, A., Puigdefábregas, C., Luterbacher, H., Fernández, M. (Eds.), Cenozoic Foreland Basins of Western Europe. Geological Society Of London Special Publication134, pp. 135–162.
North, C.P., Taylor, K.S., 1996. Ephemeral-fluvial deposits: integrated outcrop and simulation studies reveal complexity. AAPG Bulletin 80, 811–830.
Olsen, H., 1989. Sandstone-body structures and ephemeral stream processes in the Dinosaur Canyon Member, Moenave Formation (Lower Jurassic), Utah, USA. Sedimentary Geology 61, 207–221.
Ori, G., Friend, P., 1984. Sedimentary basins formed and carried piggyback on active thrust sheets. Geology 12, 475–478.
Paredes, J.M., Foix, N., Allard, J.O., Valle, M.N., Giordano, S.R., 2018. Complex alluvial architecture, paleohydraulics and controls of a multichannel fluvial system: Bajo Barreal Formation (Upper Cretaceous) in the Cerro Ballena anticline, Golfo San Jorge Basin, Patagonia. Journal of South American Earth Sciences 85, 168–190.
Parkash, B., Awasthi, A., Gohain, K., 1983. Lithofacies of the Markanda terminal fan, Kurukshetra district, Haryana, India. In: Collinson, J.D., Lewin, J. (Eds.), Modern and Ancient Fluvial Systems. IAS Special Publicationvol. 6, pp. 337–344.
Patacci, M., 2016. A high-precision Jacob's staff with improved spatial accuracy and laser sighting capability. Sedimentary Geology 335, 66–69.
Picard, M.D., High, L.R., 1973. Sedimentary Structures of Ephemeral Streams. Developments in Sedimentologyvol. 17. Elsevier, Amsterdam (223 pp.).
Plink-Björklund, P., 2015. Morphodynamics of rivers strongly affected by monsoon precipitation: review of depositional style and forcing factors. Sedimentary Geology 323, 110–147.
Puigdefàbregas, C., Muñoz, J., Vergés, J., 1992. Thrusting and foreland basin evolution in the southern Pyrenees. In: McClay, K.R. (Ed.), Thrust Tectonics. Chapman and Hall, New York, pp. 247–254.
Pujalte, V., Schmitz, B., 2005. Revisión de la estratigrafía del Grupo Tremp ("Garumniense", Cuenca de Tremp-Graus, Pirineos meridionales). Geogaceta 38, 79–82.
Pujalte, V., Schmitz, B., Baceta, J.I., 2014. Sea-level changes across the Paleocene–Eocene interval in the Spanish Pyrenees, and their possible relationship with North Atlantic magmatism. Palaeogeography, Palaeoclimatology, Palaeoecology 393, 45–60.
Pujalte, V., Schmitz, B., Payros, A., 2022. A rapid sedimentary response to the Paleocene-Eocene thermal Maximum hydrological change: new data from alluvial units of the Tremp-Graus Basin (Spanish Pyrenees). Palaeogeography, Palaeoclimatology, Palaeoecology 589, 110818. https://doi.org/10.1016/j.palaeo.2021.110818.
Reid, I., Frostick, L.E., 2011. Channel form, flows and sediments of endogenous ephemeral rivers in deserts. In: Thomas, D.S. (Ed.), Arid Zone Geomorphology: Process, Form and Change in Drylands, Third edition John Wiley & Sons, pp. 301–332.
Reineck, H.E., Singh, I.B., 1980. Depositional Sedimentary Environments: With Reference to Terrigenous Clastics. Springer-Verlag, New York.
Riera, V., Oms, O., Gaete, R., Galobart, À., 2009. The end-cretaceous dinosaur succession in Europe: the Tremp Basin record (Spain). Palaeogeography, Palaeoclimatology, Palaeoecology 283, 160–171.
Rosell, J., Linares, R., Llompart, C., 2001. El "Garumniense" prepirenaico. Revista de la Sociedad Geológica de España 14, 47–56.
Sadler, S.P., Kelly, S.B., 1993. Fluvial processes and cyclicity in terminal fan deposits: an example from the late Devonian of southwest Ireland. Sedimentary Geology 85, 375–386.
Schmitz, B., Pujalte, V., 2003. Sea-level, humidity, and land-erosion records across the initial Eocene thermal maximum from a continental-marine transect in northern Spain. Geology 31, 689–692.
Schmitz, B., Pujalte, V., 2007. Abrupt increase in seasonal extreme precipitation at the Paleocene-Eocene boundary. Geology 35, 215–218.
Schumm, S.A., 1961. Effect of Sediment Characteristics on Erosion and Deposition in Ephermeral-stream Channels. USGS Professional Paper 352-C. US Government Printing Office.
Scott, S.H., 2006. Predicting Sediment Transport Dynamics in Ephemeral Channels: A Review of Literature, DTIC Document. US Army Corps of Engineers.
Serra-Kiel, J., Canudo, J.I., Dinares, J., Molina, E., Ortiz, N., Pascual, J.O., Samsó, J.M., Tosquella, J., 1994. Cronoestratigrafía de los sedimentos marinos del Terciario inferior de la Cuenca de Graus-Tremp (Zona Central Surpirenaica). Revista de la Sociedad Geológica de España 7, 273–297.
Serra-Kiel, J., Hottinger, L., Caus, E., Drobne, K., Ferrandez, C., Jauhri, A.K., Less, G., Pavlovec, R., Pignatti, J., Samso, J.M., Schaub, H., 1998. Larger foraminiferal biostratigraphy of the Tethyan Paleocene and Eocene. Bulletin de la Société Géologique de France 169, 281–299.
Sheldon, N.D., Retallack, G.J., Tanaka, S., 2002. Geochemical climofunctions from North American soils and application to paleosols across the Eocene-Oligocene boundary in Oregon. The Journal of Geology 110, 687–696.
Sibuet, J.C., Srivastava, S.P., Spakman, W., 2004. Pyrenean orogeny and plate kinematics. Journal of Geophysical Research - Solid Earth 109, B08104. https://doi.org/10.1029/2003JB002514.
Soares, M.V.T., Basilici, G., Marinho, T.D.A., Martinelli, A.G., Marconato, A., Mountney, N.P., Colombera, L., Mesquita, A.F., Vasques, J.T., Abrantes Junior, F.R., Ribeiro, L.C.B., 2021. Sedimentology of a distributive fluvial system: the Serra da Galga Formation, a new lithostratigraphic unit (Upper cretaceous, Bauru Basin, Brazil). Geological Journal 56, 951–975.
Stanistreet, I., McCarthy, T., 1993. The Okavango Fan and the classification of subaerial fan systems. Sedimentary Geology 85, 115–133.
Stear, W.M., 1983. Morphological characteristics of ephemeral stream channel and overbank splay sandstone bodies in the Permian lower Beaufort Group, Karoo Basin. In: Collinson, J.D., Lewin, J. (Eds.), Modern and Ancient Fluvial Systems. IAS Special Publicationvol. 6, pp. 405–420.

Stear, W.M., 1985. Comparison of the bedform distribution and dynamics of modern and ancient sandy ephemeral flood deposits in the southwestern Karoo region, South Africa. Sedimentary Geology 45, 209–230.
Takano, O., Waseda, A., 2003. Sequence stratigraphic architecture of a differentially subsiding bay to fluvial basin: the Eocene Ishikari Group, Ishikari Coal Field, Hokkaido, Japan. Sedimentary Geology 160, 131–158.
Tedesco, A.M., Ciccioli, P.L., Suriano, J., Limarino, C.O., 2010. Changes in the architecture of fluvial deposits in the Paganzo Basin (Upper Paleozoic of San Juan province): an example of sea level and climatic controls on the development of coastal fluvial environments. Geologica Acta 8, 463–482.
Teixell, A., Muñoz, J.A., 2000. Evolución tectono-sedimentaria del Pirineo meridional durante el Terciario: una síntesis basada en la transversal del río Noguera Ribagorçana. Revista de la Sociedad Geológica de España 13, 251–264.
Tunbridge, I.P., 1981. Sandy high-energy flood sedimentation—some criteria for recognition, with an example from the Devonian of SW England. Sedimentary Geology 28, 79–95.
Tunbridge, I.P., 1984. Facies model for a sandy ephemeral stream and clay playa complex; the Middle Devonian Trentishoe Formation of North Devon, UK. Sedimentology 31, 697–715.
Vergés, J., Millán, H., Roca, E., Muñoz, J.A., Marzo, M., Cirés, J., Den Bezemer, T., Zoetemeijer, R., Cloetingh, S., 1995. Eastern Pyrenees and related foreland basins: pre-, syn-and post-collisional crustal-scale cross-sections. Marine and Petroleum Geology 12, 903–915.
Vyverberg, K., 2010. A Review of Stream Processes and Forms in Dry Land Watersheds. California Department of Fish and Game, Sacramento (36 pp.).
Wells, N.A., 1983. Transient streams in sand-poor red beds: Early–Middle Eocene Kuldana Formation of northern Pakistan. In: Collinson, J.D., Lewin, J. (Eds.), Modern and Ancient Fluvial Systems. IAS Special Publicationvol. 6, pp. 393–403.
Went, D.J., 2005. Pre-vegetation alluvial fan facies and processes: an example from the Cambro-Ordovician Rozel Conglomerate Formation, Jersey, Channel Islands. Sedimentology 52, 693–713.
Whitchurch, A.L., Carter, A., Sinclair, H.D., Duller, R.A., Whittaker, A.C., Allen, P.A., 2011. Sediment routing system evolution within a diachronously uplifting orogen: insights from detrital zircon thermochronological analyses from the South-Central Pyrenees. American Journal of Science 311, 442–482.
Williams, G.E., 1971. Flood deposits of the sand-bed ephemeral streams of central Australia. Sedimentology 17, 1–40.
Wilson, A., Flint, S., Payenberg, T., Tohver, E., Lanci, L., 2014. Architectural styles and sedimentology of the fluvial lower Beaufort Group, Karoo Basin, South Africa. Journal of Sedimentary Research 84, 326–348.